Quarterly Technical Report

Defects and Impurities in 4H- and 6H-SiC Homoepitaxial Layers: Identification, Origin, Effect on Properties of Ohmic Contacts and Insulating Layers and Reduction

Supported under Grant #N00014-95-1-1080
Office of the Chief of Naval Research
Report for the period 7/1/97-9/30/97

R. F. Davis, M. O. Aboelfotoh, B. J. Baliga*, R. J. Nemanich†,
M. C. Benjamin†, K. Järrendahl, S. W. King,
S. Smith, and T. Zheleva
Department of Materials Science and Engineering
*Department of Electrical and Computer Engineering
†Department of Physics
North Carolina State University
Campus Box 7907
Raleigh, NC 27695-7907

September, 1997

REPORT DOCUMENTATION PAGE

Form Approved
OMB No. 0704-0188

1. AGENCY USE ONLY *(Leave blank)*	2. REPORT DATE	3. REPORT TYPE AND DATES COVERED
	September, 1997	Quarterly Technical 7/1/97–9/30/97

4. TITLE AND SUBTITLE
Defects and Impurities in 4H- and 6H-SiC Homoepitaxial Layers: Identification, Origin, Effect on Properties of Ohmic Contacts and Insulating Layers and Reduction

5. FUNDING NUMBERS
ydl495l---01
312
N00179
N66020
4B855

6. AUTHOR(S)
R. F. Davis, M. O. Aboelfotoh, B. J. Baliga and R. J. Nemanich

7. PERFORMING ORGANIZATION NAME(S) AND ADDRESS(ES)
North Carolina State University
Hillsborough Street
Raleigh, NC 27695

8. PERFORMING ORGANIZATION REPORT NUMBER
N00014-95-1-1080

9. SPONSORING/MONITORING AGENCY NAMES(S) AND ADDRESS(ES)
Sponsoring: ONR, Code 312, 800 N. Quincy, Arlington, VA 22217-5660
Monitoring: Administrative Contracting Officer, Atlanta Regional Office
Office of Naval Research
100 Alabama Street, Suite 4R15
Atlanta, GA 30303

10. SPONSORING/MONITORING AGENCY REPORT NUMBER

11. SUPPLEMENTARY NOTES

12a. DISTRIBUTION/AVAILABILITY STATEMENT
Approved for Public Release; Distribution Unlimited

12b. DISTRIBUTION CODE

13. ABSTRACT ***(Maximum 200 words)***

Aluminum nitride (AlN) thin films with very smooth surfaces have been grown by gas-source molecular beam epitaxy on 4H- and 6H-SiC substrates. Streaked reflection high energy electron diffraction patterns and reconstructions of the AlN surfaces indicated smooth films. Atomic force microscopy (AFM) and transmission electron microscopy (TEM) showed root mean square values ≤1 nm and very flat surfaces, respectively. X-ray diffraction showed the films to be highly c-axis oriented and single phase. Major impurities in the AlN films were oxygen and carbon, as revealed by secondary ion mass spectrometry. A correlation has been found between the types and the distributions of the dominant defects, namely, micropipes and screw dislocations using optical microscopy, scanning electron microscopy, AFM, synchrotron white beam x-ray topography, and electron beam induced current (EBIC) studies. A ridge-type structure of the core of the micropipes, related to the growth front flow direction was observed with AFM. Triangular micro inclusions associated with the cubic 3C-SiC polytype (β-SiC) were detected. EBIC studies revealed various types of electrically active defect regions, related to the β-SiC phase and randomly distributed within the wafers and across different Shottky diodes. X-ray photoelectron spectroscopy, Auger electron spectroscopy (AES), low energy electron diffraction (LEED), and temperature programmed desorption (TPD) revealed that exposure of 6H-SiC to atomic hydrogen selectively removes Si from the surface and converts the (3×3) surface to a (1×1) surface. Additional etching of this surface was indicated by the reduction in the Si LVV/C KLL ratio in AES from 1.3 to 0.4 following exposure of (3×3) surfaces to a remote rf H plasma. TPD of atomic H treated (3×3) SiC surfaces showed weak hydrogen desorption in the range of 400-600°C where desorption from Si atoms would be expected by analogy to (111) Si. However, the hydrogen desorption signal increased at higher temperatures where hydrogen desorption from carbon sites would be expected based on analogy to (111) diamond surfaces. C-H termination of the SiC surface was supported by the observation of some C-C bonding after thermal desorption of rf plasma treated SiC surfaces at T > 1000°C.

14. SUBJECT TERMS
AlN, SiC, gas-source molecular beam epitaxy, reflection high energy electron diffraction, atomic force microscopy, transmission electron microscopy, secondary ion mass spectrometry, optical microscopy, atomic force microscopy, synchrotron white beam x-ray topography, electron beam induced current, micropipes, screw dislocations, Auger electron spectroscopy, low energy electron diffraction

15. NUMBER OF PAGES
37

16. PRICE CODE

17. SECURITY CLASSIFICATION OF REPORT	18. SECURITY CLASSIFICATION OF THIS PAGE	19. SECURITY CLASSIFICATION OF ABSTRACT	20. LIMITATION OF ABSTRACT
UNCLAS	UNCLAS	UNCLAS	SAR

NSN 7540-01-280-5500

Standard Form 298 (Rev. 2-89)
Prescribed by ANSI Std Z39-18
298-102

Table of Contents

I. Introduction

The two most important materials-related problems affecting the performance of all SiC devices and their associated components (e.g., contacts) are the defects and the undesired impurities which become incorporated in the homoepitaxial SiC layers in which all devices are currently fabricated. Bhatnagar [1] has shown that the reverse blocking leakage current in high voltage Schottky diodes is three orders of magnitude higher than theoretically predicted as a result of defects in the epi-layer. The formation of micropipes, stepped screw dislocations, interacting dislocation loops, polyganized networks of dislocations and growth twins as well as stacking faults during the sublimation growth of SiC boules are likely the root cause of some of the defects in the epitaxial layer. However, with the exception of the micropipes, the types and concentrations of line, planar and other three-dimensional defects and their effect on the performance of devices and individual device components in the important epi-layer have not been similarly determined. As such, it is not known which of the latter defects actually are translated from the wafer into the epi-layer during its deposition and, therefore, should be vigorously controlled during boule growth and which defects are generated during deposition.

The relatively uncontrolled occurrence of the n-type donor of N and deep level compensating impurities such as Ti in the epilayer have been identified via secondary ion mass spectrometry, photoluminescence and cathodoluminescence investigations. However, the origins of essentially all of these impurities are unknown. For high-temperature, -power and -frequency devices, it is highly desirable to control or eliminate these impurities such as to attain undoped films with uncompensated carrier concentrations of 10^{14} cm^{-3}—two orders of magnitude lower than what is, at present, normally achieved in standard commercial depositions.

The formation of low resistivity and thermally stable ohmic contacts to 4H- and 6H-SiC remains a serious problem in the development of SiC device technology. For SiC power devices to have an advantage over Si, the contact resistivities must be below 1×10^{-5} W-cm^2, as noted by Alok, *et al.* [2]. In addition, the electrical characterization of state-of-the-art SiC films depends on the ability to fabricate ohmic contacts on material with low carrier concentrations. Therefore, better ohmic contacts are needed both for improving device performance and for improving the quality of films which can be grown. The thermal stability of ohmic contacts is of particular concern for p-type SiC, which have traditionally relied on low melting point Al or Al alloys to dope the SiC surface below the contacts. These materials are not suitable for devices intended for high-temperature operation. While the fabrication of ohmic contacts to SiC has also normally depended on the attainment of a very heavily-doped near-surface region, the introduction during deposition of high levels of dopants in the near surface device region of the epi-layer prior to the deposition of the contact or by ion implantation through the contact makes probable the introduction of point and line defects as a result of the induced strain in the lattice.

Based on all of these issues and recent experiments already performed at NCSU, our goals are to produce contacts which are thermally stable and have low contact resistivities while also reducing the need for doping by ion implantation.

To fabricate most microelectronic devices, the growth or deposition of stable insulators is needed to provide both passivating layers and gate dielectrics. Silicon carbide is almost invariably thermally oxidized, albeit at a slower rate, in the same manner and temperature range that is employed for Si. Most of the previous studies regarding the oxidation of SiC have been concerned with polycrystalline materials. It has been shown by Harris and Call [3] and Suzuki, *et al.* [4] that the (0001) face of 6H-SiC oxidizes according to the same linear-parabolic equation reported for Si by Deal and Grove [5]. The model states that the initial stage of oxidation is reaction rate limited and linear, but becomes parabolic as the diffusion of the oxidant through the oxide becomes the rate limiting factor. Research at NCSU by Palmour, *et al.* [6] has demonstrated that the oxidation process on SiC in wet and dry oxygen and wet argon obeys the linear-parabolic law. Both wet processes had a slower rate than dry oxidation at 1050°C and below. The dry oxides exhibited a very flat surface; in contrast, SEM and TEM revealed that wet oxidation preferentially oxidizes dislocation bands, causing raised lines on the oxide and corresponding grooves in the SiC. It was proposed that the much higher solubility of H_2O in SiO_2 as compared to that of O_2 allows wet oxidation to be preferential.

All of the oxidation studies on all polytypes of semiconductor quality SiC have been conducted on n-type material with the exception of the investigation by Palmour *et al.* [6]. The objective of this study was the determination of the redistribution of the common electrical dopants of N, P, Al and B during thermal oxidation of SiC films at 1200°C in dry O_2. Experimental segregation coefficients and interfacial concentration ratios were determined. Secondary ion mass spectrometry revealed that B and Al depleted from the SiC into the growing oxide while N and P were found to pile up in the SiC as a result of the loss of the SiC to the oxide formation. Aluminum is now used almost universally as the p-type dopant in SiC. The electrical properties of oxides thermally grown on n-type SiC normally have reasonably favorable characteristics of high breakdown voltage and low leakage currents. However, the reverse is true for thermally grown oxides on p-type SiC, as shown by Baliga and his students at NCSU. It is believed that at least two of the causes of the poor performance on a p-type material are the existence of the Al in the oxide and at the oxide/SiC interface and the dangling oxygen bonds which this species creates in the oxide as a result of a difference in oxidation state (+3) compared to that of Si (+4) and the existence of C at the SiC/insulator interface. Methods of effectively cleaning SiC surfaces prior to oxidation to deposit and grow oxides on p-type material under UHV conditions and determine the effect of Al redistribution and C concentrations at the interface on the properties of the oxide must be determined. In addition,

the effect of existing line and planar defects in the SiC epi-layer on the properties of the thermally grown and deposited oxide must be ascertained.

The research conducted in this reporting period and described in the following sections has been concerned with (1) the determination and employment of an effective, completely dry, *ex situ* hydrocarbon and oxide removal process for the 6H-SiC(0001) surface, (2) design and construction of a new CVD SiC system for the deposition and doping of 6H- and 4H-SiC and AlN films, (3) deposition, annealing and electrical characterization of Ni, NiAl, Au, Pt and Cr-B contacts to p-type SiC(0001), and (4) fabrication, for the first time, of high voltage Schottky barrier diodes on 4H- and 6H-SiC(0001) and determination of the associated barrier heights, series resistance and critical electric field strength for breakdown as a function of T. The following individual sections detail the procedures, results, discussions of these results, conclusions and plans for future research. Each subsection is self-contained with its own figures, tables and references.

References

1. M. Bhatnagar, Ph. D. Thesis, North Carolina State University, 1994.
2. D. Alok, B. J. Baliga and P. K. McLarty, IEDM Technical Digest, IEDM 1993, 69 (1993).
3. R. C. A. Harris and R. L. Call in *Silicon Carbide–1973*, R. C. Marshall, J. W. Faust and C. E. Ryan, Eds. University of South Carolina Press, Columbia, S. C., 1974, p. 534.
4. Suzuki, *et al.*, Jap. Journ. Appl. Phys. **21**, 579 (1982).
5. B. E. Deal and A. S. Grove, J. Appl. Phys. **36**, 3770 (1965).
6. J. W. Palmour, R. F. Davis, H. S. Kong, S. F. Corcoran and D. P. Griffis, J. Electrochem. Soc. **136**, 502 (1989).

II. Growth of SiC and AlN by Gas-Source Molecular Beam Epitaxy

A. Introduction

Due to its low dielectric constant and close lattice match to SiC, AlN may be an alternative to silicon dioxide (SiO_2) as a dielectric in high-power and high-temperature SiC devices. Highly (0001)-oriented AlN has been fabricated using reactive magnetron sputtering [1,2], gas-source molecular beam epitaxy (GSMBE) [3], chemical vapor deposition (CVD) [4], and "hot wall" CVD [5]. However, the material contains high densities of line defects and high concentrations of oxygen and carbon. It is also important to reduce the surface roughness of the AlN. This report presents recent results [6,7] concerning the growth of AlN by GSMBE using NH_3 as the nitrogen source. It is shown that highly c-axis oriented wurtzite AlN films with very smooth surfaces can be grown on 4H and 6H-SiC substrates.

B. Experimental Procedure

The growth is conducted in a GSMBE system with an ultimate base pressures of 10^{-10} Torr. Prior to growth, SiC substrates are cleaned using procedures developed at NCSU [3]. The SiC films are grown using Si_4 and C_2H_4 where the gas flows are accurately controlled by regulating the pressure over a flow cell. The AlN growth is made by evaporating Al from an effusion cell and simultaneously introducing NH_3 through a mass flow controller. In addition to the gases mentioned above, it is also possible to introduce H_2, N_2 and Ar during growth. The system is equipped with two *in situ* analysis tools. The gases in the chamber are monitored with a 100 AMU residual gas analyzer (RGA). Differential pumping of the RGA makes it possible to record the gas content in the chamber at pressures above 1×10^{-3} Torr. The surface structures are analyzed with reflection high energy electron diffraction (RHEED).

In addition to these *in situ* techniques, several *ex situ* analysis techniques are available, for instance, transmission electron microscopy (TEM), x-ray diffraction (XRD), scanning electron microscopy (SEM) and atomic force microscopy (AFM) for structural investigations, Auger electron spectroscopy (AES) and secondary ion mass spectroscopy (SIMS) for chemical analysis.

C. Results and Discussion

The RHEED patterns from the AlN surfaces indicated that very smooth films were grown on all types of SiC substrates. This was particularly true for the films grown on the on-axis 4H-SiC(0001), 4H-SiC ($000\bar{1}$), and 6H-SiC(0001) substrates. The patterns were very streaked and showed Kikuchi lines. Along $<1\bar{1}00>$, additional streaks were seen due to reconstruction of the AlN surface which also implied that the films had very smooth surfaces. The RHEED pattern can be interpreted as a $(\sqrt{3}\times\sqrt{3})R30°$ reconstruction. The two reconstruction streaks observed only in the $<1\bar{1}00>$ pattern were also typical for growth on the

vicinal surfaces and C-faced on-axis surfaces. In some cases, however, additional weak reconstruction streaks were seen in the <1$\bar{1}$00> patterns indicating some other type of reconstruction. Another possibility is that the ($\sqrt{3}\times\sqrt{3}$)R30° reconstruction coexists with a second type of reconstruction. Reconstructed AlN surfaces were, to the author's best knowledge, reported for the first time [6,7].

Measurements via AFM confirmed that the AlN surfaces were smooth. The root mean square (RMS) value of the surface roughness were below 1 nm for all measured samples in this work. Cross sections of the samples investigated by TEM showed very flat surfaces in agreement with the RHEED and AFM results. The films had a domain structure with mismatch boundaries which is common for AlN films. A highly c-axis oriented structure and no secondary phases were observed using XRD. SIMS measurements of the levels of oxygen, carbon and silicon showed that the concentration of all these materials were high. For instance, the lowest concentration of oxygen in the GSMBE grown films were ~10^{19} cm^{-3}.

D. Future Research Plans and Goals

Presently the RHEED, RGA, TEM, XRD, and SIMS data from the AlN films are being analyzed. This will result in more detail regarding the GSMBE growth of AlN.

The previous research [8-10] on GSMBE deposition of SiC on 6H-SiC substrates will be continued. Investigations regarding the mechanisms controlling the surface chemical effects of H_2 on SiC growth rate and polytype change (3C to 6H) will be investigated in more detail. The experiments will also be conducted on 4H-SiC substrates. A goal in this research is to investigate the possibilities to deposit 6H or 4H-SiC on 3C-SiC and wurtzite AlN.

E. References

1. K. Järrendahl, J. Birch, L. Hultman, B. Pécz, G. Radnoczi, J.-E. Sundgren, and J. E. Greene, In manuscript.
2. S. Tungasmita, J. Birch, L. Hultman, E. Janzén, and J.-E. Sundgren, In manuscript.
3. R. S. Kern, Thesis, Dept. of Materials Science and Engineering, North Carolina State University, Raleigh, 1996.
4. T. W. Weeks, M. D. Bremser, K. S. Ailey, E. P. Carlson, W. G. Perry, E. L. Piner, N. A. El-Masry, and R. F. Davis, *J. Mater. Res.* **11**, 1081, 1996.
5. U. Forsberg, J. Birch, M.F. MacMillan, P.O.Å. Persson, and E. Janzén, In manuscript.
6. K. Järrendahl, S. Smith, T. Zheleva, and R. F. Davis, in the *Proceedings from the International Conference on Silicon Carbide, III-Nitrides and Related Materials*, Stockholm, August 31 - September 5, 1997, accepted for publication.
7. K. Järrendahl, S. Smith, T. Zheleva, and R. F. Davis, submitted to Vacuum.
8. R. S. Kern, K. Järrendahl, S. Tanaka and R. F. Davis, Phys. Stat. Sol. (b) **202**, 379, 1997.
9. R. S. Kern, K. Järrendahl, S. Tanaka and R.F. Davis, Diamond and Related Materials **6**, 1282, 1997.
10. R. S. Kern, S. Tanaka, L. B. Rowland, and R. F. Davis, J. Cryst. Growth, accepted for publication.

III. Defects in Silicon Carbide Homoepitaxial Layers

A. Introduction

The advantages of SiC-based devices for numerous applications in optoelectronics, high-temperature electronics, radiation resistance electronics, and high-power/high-frequency electronics [1,2] are impeded by the various materials-related problems, such as the defects and the impurities incorporated in the homoepitaxial SiC layer during the devices fabrication. Most of the defects in the SiC epilayers originate from the corresponding defect structures in the SiC wafers. The defects present in the SiC wafers have been studied by various groups [3-5]. It was found that the screw dislocations, micropipes and the subgrain boundaries are the predominant defects in the SiC wafers. It is recognized that the critical issues for the wafer quality are the stages of crystal growth, polishing, epilayer growth and the postgrowth processing of the devices [6]. Therefore, the primary mechanisms for the formation of the major defects, micropipes or super-screw dislocations in the SiC wafers, can be classified as [7]: (i) fundamental—a) thermodynamic (thermal field uniformity, dislocation formation, solid state transformation, vapor phase composition, vacancy supersaturation) and b) kinetic (nucleation process, inhomogenious supersaturation, constitutional supercooling, growth face morphology, capture of gas phase bubbles), and (ii) technological—related to the process instabilities, seed preparation, and the contamination. It has been found that most of the wafer growth defects can be eliminated and/or reduced significantly by epilayer film growth. Thus, for device operation, the most important defects are the ones existing in the epilayer. The objective of the presented investigations is to (i) identify the defects present in 4H-SiC homoepitaxial films and compare their type and distribution with that in the SiC wafers; (ii) determine the material origin of these defects; and (iii) correlate the type, density and distribution of defect with the electrical properties of a device.

B. Experiment

To obtain information about the defects and the difference in their type and distribution across the SiC wafers without an epilayer and with an epilayer, two types of samples were investigated: (i) 4H-SiC wafers, with 8° off-cut angle, and (ii) 4H-SiC wafers, 8° off-cut, with 5 μm thick 4H-SiC epilayer [8]. To study the effect of the defects on device operation, circular Ti Schottky diodes were fabricated on the above two types of wafers with diameters 50 μm, 100 μm, 150 μm, and 200 μm. The wafers were characterized for crystalline quality before and after device fabrication. Optical microscopy (Nomarski OM) was used to reveal the overall surface morphology. Scanning electron microscopy (SEM) and atomic force microscopy (AFM) were used to image the surface morphology and the cores of the micropipes and the screw dislocations. Synchrotron white beam x-ray topography (SWBXT) experiments

in transmission, reflection and diffraction modes, were performed at the Beamline X-19C at the NSLS in Brookhaven National Laboratory to characterize the crystalline quality of the samples. Electron beam induced current (EBIC) experiments were performed with a SEM microscope equipped with EBIC attachment to characterize the electrically active regions throughout the Schottky device structures.

C. Results and Discussion

Examination of the surfaces of the 4H-SiC wafers with Nomarski OM revealed the overall morphology of the surfaces of the two types of samples. Common to the two types of surfaces was the non-uniform distribution of the defects which were with higher density closer to the edges of the wafers at a distance ~ one fourth to one third of the wafers radius. The density of the defects at the central regions was lower. Most of the defects on the 4H-SiC wafers were microcracks with random orientation, micropipes with radius few to tens microns, and growth pits [9-11], as shown in Fig. 1a. The surfaces of the wafers with epilayers were free of microcracks, but the micropipes and the pits were present, as shown in Fig. 1b.

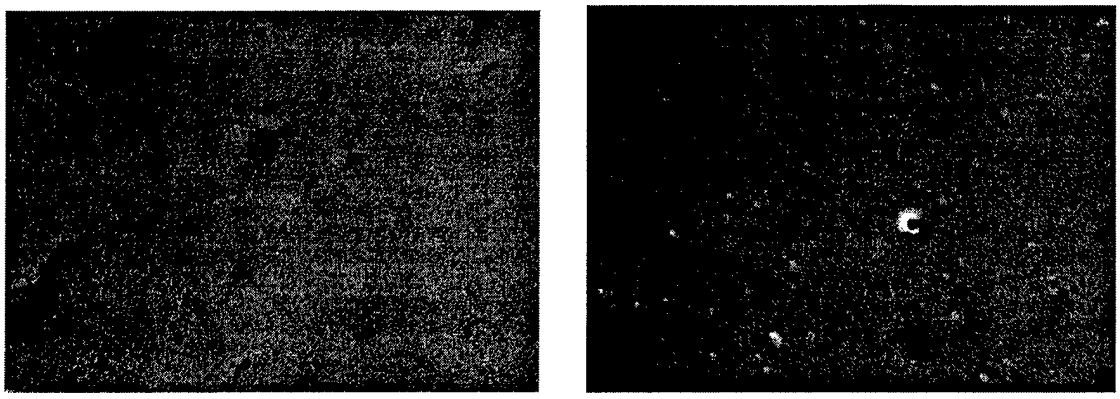

a) b)

Figure 1. Nomarski OM from 4H-SiC wafers a) without an epilayer and b) with 5 μm 4H-SiC epilayer.

The morphology of the surfaces of the wafers and particularly that near the defects structures was studied by SEM and AFM, which revealed the non-uniform defects distribution throughout the surfaces. It was interesting to note the predominantly ridge-like type structure of the core of the micropipes in the 4H-SiC wafers with epilayer, revealed from the SEM and AFM observations, as shown in Fig. 2. The directionality of these ridges is primarily along [10-19] which is the growth front flow direction. Thus, the core of the predominant defect structures in the 4H-SiC is filled on-uniformly and, therefore, is an unwanted template for

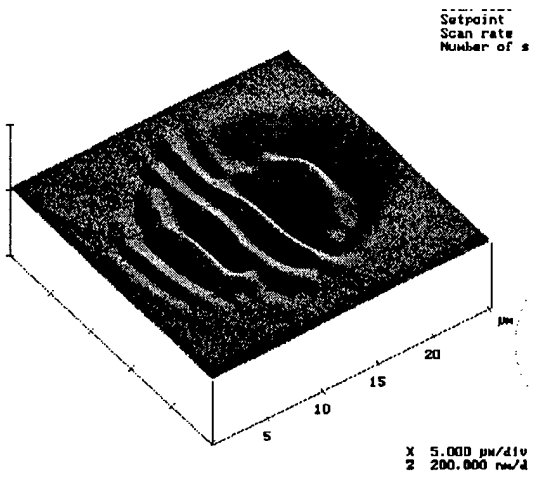

Figure 2. AFM image of a core of a micropipe with filled ridge-like structure from a 4H-SiC wafer with an epilayer.

the devices to be grown on top of it. On many occasions, the micropipes are adjacent to each other meaning that these superscrew dislocations most probably have opposite Burgers vectors [12].

It is shown that SWBXT is particularly useful for revealing the configurations of crystalline defect structures and mixed phases in large areas [13, 14]. The advantages of the synchrotron radiation as low divergence -2×10^{-4} radians in the vertical plane, high intensity, excellent geometrical resolution ~0.04 μm per cm of the specimen to film distance provide precise structural information for the defects distribution in transmission and reflection geometry. In diffraction geometry, each large area diffraction spot represents a map of the diffracting power from a particular set of planes as a function of the position in the crystal with excellent point-to-point resolution. Thus, each diffraction spot is x-ray topograph from that diffracting particular crystal area. X-ray topography experiments in transmission and reflection settings showed, in agreement with other studies on 4H-SiC and 6H-SiC, that the dominant defects in the 4H-SiC wafers are the micropipes, identified as hollow core screw dislocations with multiple Burgers vector of size 2-10c, where c is the lattice parameter of SiC in [0001] direction [15-19], as seen from Fig. 3. The micropipes with varying size are non-uniformly distributed across the wafers as their density is again higher near the edges. Growth pits are also readily observed across the areas, and their density is higher in the wafers with epilayer. A large portion of the defect structures in the 4H-SiC wafers without epilayer revealed by SWBXT are the domain boundaries which are very few in the 4H-SiC wafers with epilayer. Synchrotron white beam x-ray topography in the diffraction mode taken from the center of the wafers with fabricated Schottky device structures revealed triangular defects [11] which have been identified to exist in 6H-SiC and 4H-SiC epilayers as the cubic 3C-SiC (β-SiC) phase [20].

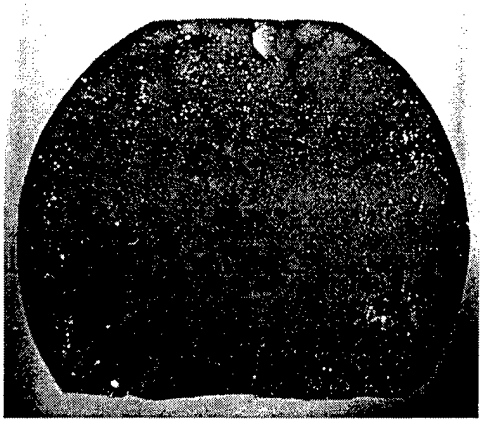

Figure 3. SWBXT image in transmission mode of a 4H-SiC wafer with 4H-SiC epilayer. Micropipes are readily seen as white circles predominantly closer to the edges of the wafer.

Electron beam induced current studies were performed on Schottky device structures to reveal the electrically active regions across the wafer surface. In this technique, the charge carriers generated by the electron beam of the microscope are collected by the electric field within the material and sensed as a current in the external circuit. When employed as a video signal of the SEM, this collected current image reveals inhomogeneities in the electrical properties of the material. Electron beam induced current studies revealed that the electrically active defect-related centers display three types of contrast shape: (i) circular, (ii) single line or line clusters, and (iii) large triangular shapes, as shown in Fig. 4. The circular pattern with varying size in the EBIC image can be associated with the open micropipes or the superscrew dislocations, revealed by all other characterization techniques. The line and line cluster defects can be associated possibly with the ridge-like structure of the closed micropipes. The large triangular defects can be associated with the 3C-SiC inclusions in the 4H-SiC epilayer as studied extensively by SWBXT [20]. Also, the 4H-SiC wafers without epilayer revealed lower defects density compared to the wafers with epilayer. Increase of the electron beam voltage from 5 to 30 kV, at a step of 5 kV, i.e. increase of the penetration depth of the electrons, enhances the contrast from these triangular defects, revealing that they originate deeper from the epitaxial film surface in the vicinity of the interface region. This is in agreement with the observations from other researchers that the 3C-SiC phase can be formed at the 4H-SiC epi/4H-SiC wafer interfaces when the step-flow mode is disturbed.

Attempts will be made to correlate the triangular defects observed with EBIC, SWBXT, and TEM to proof their β-SiC nature and reveal their origin. The origin for the strong electrical activity of these defects has to be determined, as well.

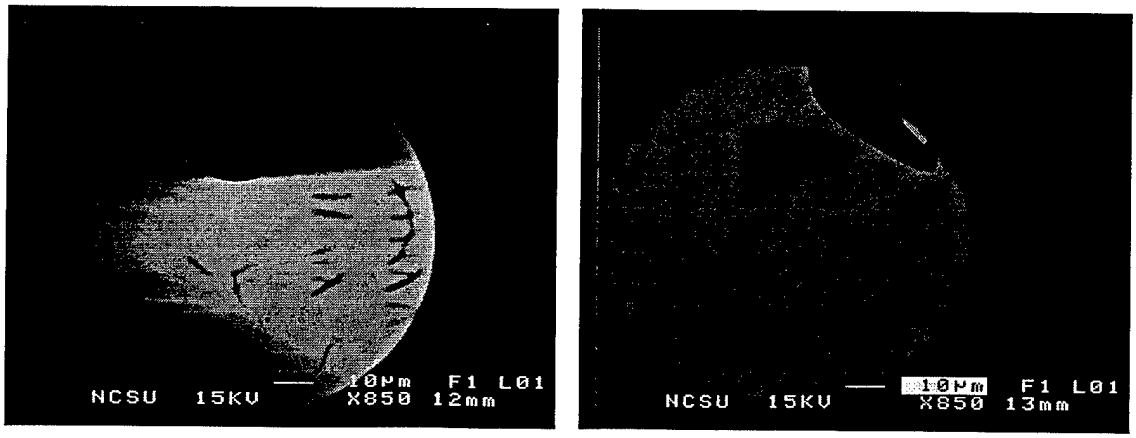

a) b)

Figure 4. EBIC images from 4H-SiC wafer a) without epilayer and b) with 4H-SiC epilayer.

D. Summary

Various characterization techniques have been employed to analyze the morphology and crystal structure quality of the 4H-SiC wafers. It was found from all characterization studies that the dominant defects are the micropipes or super screw dislocations with Burgers vectors 2-10c. They are distributed non-uniformly across the surface with lower density at the center. Most of the micropipes are with closed ridge-type cores, as revealed with SEM and AFM. Inclusions from a second phase present in the 4H-SiC epilayers, which can be associated with the cubic β-SiC phase as revealed from SWBXT. The strong triangular contrast from the EBIC images suggests that these triangular defects are extremely electrically active, as the electrical activity is stronger closer to the 4H-SiC epi/4H-SiC wafer interface. The source of this electrical activity has yet to be determined.

E. Acknowledgments

The efforts and valuable discussions with Prof. M. Dudley and Dr. W. Si from SUNY at Stoney Brook for SWBXT studies are gratefully acknowledged. Collaboration with Dr. Z. Radzhimsky, Dr. D. Bachelor and Dr. M. Tomita with the EBIC studies is gratefully appreciated.

F. References

1. H. Morcoç, S. Strite, G. Gao, M. Lin, B. Sverdlov, and M. Burns, J. Appl. Phys. **76** (3), 1363 (1994).
2. J. W. Palmour, J. A. Edmond, H.-S. Kong, and C. H. Carter, Jr., in *Amorphous and Crystalline Silicon Carbide IV*, Ed. C. Y. Yang, M. M. Rahman, G. L. Harris, Springer Proceedings in Physics **71**, Springer-Verlag (1992) pp. 289-297.
3. D. L. Barrett, J. P. McHugh, H. M. Hobgood, P. G. McMullin, R. C. Clarke and W. J. Choyke, J. Cryst. Growth **128**, 358 (1993).

4. H. M. Hobgood, J. P. McHugh, J. Greggi and R. H. Hopkins in *Silicon Carbide and Related Compounds*, M. G. Spencer *et al.* eds., Inst. of Physics Conference Series No. 137, Inst. Phys. Publ., Philadelphia, PA (1994), pp. 7-12.
5. J. A. Powel, P. G. Neudek, D. J. Larkin, J. W. Yang and P. Pirouz, in *Silicon Carbide and Related Compounds*, M. G. Spencer *et al.* eds., Inst. of Physics Conference Series No. 137, Inst. Phys. Publ., Philadelphia, PA (1994), pp. 161-164.
6. C. Carter, Silicon Carbide High-Power Electronic Materials Program Review, Arlington, VA, 1997.
7. V. F. Tsvetkov, S. T. Allen, H. S. Kong, and C. H. Carter, Jr., Proc. Int. Conf. on SiC and Related Materials, Sept. 18-21, 1995, Kyoto, Japan in *Silicon Carbide and Related Compounds*, M.G. Spencer *et al.* Eds., Inst. of Physics Conference Series No. 137, Inst. Phys. Publ., Philadelphia, PA (1994), pp. 7-12.
8. CREE Research, Inc.
9. C. Carter, Silicon Carbide High-Power Electronic Materials Program Review, Arlington, VA, 1997.
10. A. R. Powel, N. Baba-Ali, S. Wang, G. R. Brandes, and D. W. Brown, Silicon Carbide High-Power Electronic Materials Program Review, Arlington, VA, 1997.
11. J. A. Powell, D. Larkin, P. Neudeck, A. Trunek, Silicon Carbide High-Power Electronic Materials Program Review, Arlington, VA, 1997.
12. J. P. Hirth and J. Lothe, *Theory of Dislocations,* John Wiley & Sons, 1982.
13. M. Dudley, Mat. Res. Soc. Symp. Proc. **307**, 213-224 (1993).
14. B. K. Tanner, *X-Ray Diffraction Topography*, Pergamon Press 1976.
15. S. Wang, M. Dudley, C. Carter, Jr., D. Asbury, and C. Fazi, Mat. Res. Soc. Symp. Proc., **307**, 249-253 (1993).
16. M. Huang, S. Wang, M. Dudley, P. Neudeck, J. A. Powell, and C. Fazi, Mat. Res. Soc. Symp. Proc. **375**, 313-318 (1995).
17. M. Dudley, W. Huang, S. Wang, J. A. Powell, P. Neudeck, and C. Fazi, J. Phys. D: Appl. Phys. **28** A56-A-62 (1995).
18. M. Dudley, S. Wang, W. Huang, C. Carter Jr., V. Tsvetkov, and C. Fazi, J. Phys. D: Appl. Phys. **28** A63-A68 (1995).
19. W. Si, M. Dudley, R. Glass, V. Tsvetkov, and C. Carter, Jr., J. Electronic Materials **26** No. 3, 128 (1997).
20. W. Si, M. Dudley, H.-S. Kong, J. Sumakeris, and C. Carter, Jr., J. Electronic Materials **26** No. 3, 151 (1997).

IV. Interaction of Atomic Hydrogen with (3×3) 6H-SiC $(0001)_{Si}$ Surfaces

Sean W. King, *Mark C. Benjamin, John P. Barnak,
*Robert J. Nemanich, and Robert F. Davis

Department of Materials Science and Engineering
*Department of Physics
North Carolina State University
Raleigh, NC 27695

Abstract

X-ray photoelectron spectroscopy (XPS), Auger electron spectroscopy (AES), low energy electron diffraction (LEED), and temperature programmed desorption (TPD) were used to examine the interaction of atomic hydrogen with (3×3) 6H-SiC $(0001)_{Si}$ surfaces. It was found that atomic hydrogen exposure selectively removes silicon from the SiC surface converting the (3×3) surface to a (1×1) surface. Selective removal of silicon was witnessed by the reduction and removal of the Si-Si bonding Si 2p XPS peak from (3×3) $(0001)_{Si}$ 6H-SiC surfaces exposed to atomic hydrogen. Additional etching of the SiC surface was indicated by the reduction in the Si LVV/C KLL ratio in AES from 1.3 to 0.4 following exposure of (3×3) surfaces to a remote rf H plasma. TPD of atomic H treated (3×3) SiC surfaces showed weak hydrogen desorption in the range of 400-600°C where desorption from silicon atoms would be expected by analogy to (111) Si. However, the hydrogen desorption signal increased at higher temperatures where hydrogen desorption from carbon sites would be expected based on analogy to (111) diamond surfaces. C-H termination of the SiC surface was supported by the observation of some C-C bonding after thermal desorption of rf plasma treated SiC surfaces at T > 1000°C.

Submitted to Surface Science

I. Introduction

Hydrogen is a common constituent in many semiconductor processes including chemical vapor deposition (CVD), reactive ion etching (RIE), wet chemical cleaning, gas source molecular beam epitaxy (GSMBE), and rapid thermal annealing (RTA) [1-12]. Knowledge of the interaction and chemistry of hydrogen at semiconductor surfaces is, therefore, of great importance in order to understand the fundamentals of the above processes. For these reasons, many surface analytical studies concerned with the interaction of hydrogen with semiconductor surfaces such as silicon, diamond, and gallium arsenide [13-46] have been conducted. However, there have been relatively few surface analytical studies concerned with the interaction of hydrogen and silicon carbide (SiC) [47-51]. Silicon carbide is a wide band gap semiconductor (E_g (6H-SiC) = 3.0 eV) which is of interest for high-power, high-frequency, and high-temperature electronic devices due to its excellent oxidation resistance, high saturation electron drift velocity ($v_{sat} = 2\times10^7$ cm/s), high breakdown voltage (E_B = 2.5 MV/cm), high thermal conductivity (κ = 4.9 W/cm K), and high melting point ($T_{melt} \approx 3000°C$) [52,53]. Due to moderately close lattice matching ($\Delta a/a_0$ AlN/SiC = 0.8%, GaN/SiC = 3.5%), SiC is also of interest as a heteroepitaxial substrate for growth of III-V nitride compounds which in turn are of interest for blue/UV optoelectronic applications, as well as high-power and high-frequency devices [54]. Unfortunately, many of the same properties which make SiC of interest in these demanding conditions also makes it a challenging material to work with from a processing point view. Therefore, in order for SiC to succeed in many of these applications, advances must be made in SiC processing such as growth, etching, contact formation, and surface cleaning [52]. As many of these processes are currently based on using hydrogen or hydrogenated species, an increased understanding of the interaction of hydrogen with SiC surfaces should assist in the further development of these processes.

Some of the first investigations of the interaction of hydrogen with SiC revealed that etching of SiC by hydrogen occurred at high temperatures (>1500°C) [55-58]. The work of Chu and Campbell [55] in particular found hydrogen to be a non-preferential etchant for single crystal hexagonal SiC yielding useful etch rates of 2-4 microns/min. at temperatures of 1600-1700°C. Further, Bartlett and Mueller [57], found an H_2 etch prior to SiC CVD to be instrumental in obtaining good homoepitaxy. Subsequent hydrogen/SiC studies focused on the interaction of high energy H^+ and D^+ ions (i.e. sputtering and implantation) with polycrystalline 3C-SiC which in these studies was being considered as a first wall material for thermonuclear fusion reactors [59-65]. However, more recent studies have investigated the interaction of low energy (i.e. thermally generated) atomic hydrogen with polycrystalline 3C-SiC surfaces [47-48]. The first such study by Allendorf *et al.* [47] used temperature programmed desorption (TPD) and Auger electron spectroscopy (AES) to investigate the adsorption and desorption of thermally generated hydrogen on sputter cleaned polycrystalline

3C-SiC surfaces. They observed > 1 ML adsorption of hydrogen which was observed via TPD to desorb in a broad temperature range from 400-1000°C. Analysis of the broad desorption feature indicated two desorption peaks at 700 and 850°C characterized by first order desorption with activation energies of 63 and 72 kcal/mole, respectively. Due to the polycrystalline nature of these surfaces, Allendorf *et al.* [47] unfortunately were not able to assign these two desorption features to desorption from specific sites. However, they did show a reduction in the AES Si/C ratio from 1.31 to 0.46 after atomic H exposure suggesting etching or selective etching of the SiC surface. A similar effect was observed by Lannon *et al.* [49] for polycrystalline 3C-SiC films exposed to $(H/H_2)^+$ ions of various energies (10-2000 eV). In this case, the 3C-SiC films were grown *in situ* via carbonization of (001) silicon wafers with C_2H_4 and were not exposed to any sputtering. Finally, the reaction of thermally generated atomic hydrogen with polycrystalline 3C-SiC films was also studied by Kim and Olander [48] using modulated molecular beam mass spectrometry. In this case, they were able to observe etching of SiC by atomic hydrogen at temperatures ranging from 300-1100K via the detection of SiH_4, CH_4, and C_2H_2 reaction products. Based on their study and those of Allendorf *et al.* [47], Kim and Olander proposed a precursor model for SiH_4 and CH_4 formation based on a surface composed of adsorbed atomic hydrogen overlaying mono and dihydrides of silicon and carbon on the SiC surface. In their model, the dihydrides act as the precursors for SiH_4 and CH_4 generation and the production of these species follows a first order reaction between dihydrides and the overlayer of adsorbed atomic hydrogen. However, the results of Kim and Olander and those of Kim and Choi [58] showed pronounced and enhanced etching of polycrystalline 3C-SiC surfaces at grain boundaries suggesting that their results may be more indicative of processes occurring at grain boundaries rather than at crystalline surfaces. Therefore, in this study we have chosen to examine the reaction of atomic hydrogen with single crystal (3×3) reconstructed $(0001)_{Si}$ 6H-SiC surfaces.

The (3×3) reconstructed $(0001)_{Si}$ 6H-SiC surface is rapidly becoming a well-characterized semiconductor surface [66-73] and common starting point for most MBE growth of SiC, AlN, and GaN on $(0001)_{Si}$ 6H-SiC substrates [73-75]. This surface has been shown to consist of an incomplete bilayer of silicon overlaying the SiC surface [66-68,76]. In addition, STM investigations have shown this bilayer to be arranged in a structure similar to the (7×7) Si (111) DAS model [70-72]. In our case, this surface was prepared by chemical vapor cleaning processes and was not exposed to sputtering processes which are known to create a number of surface defects which can control surface chemistry. Surface analytical techniques such as UV and x-ray photoelectron spectroscopy (UPS and XPS), Auger electron spectroscopy (AES), low energy electron diffraction (LEED), and temperature programmed desorption (TPD) were used to study not only the effects of atomic hydrogen on the chemistry of SiC surfaces but on

the electronic structure of (3×3) 6H-SiC $(0001)_{Si}$ surfaces, as well. The details of the effect on the electronic structure, however, will be presented in a separate paper [77].

In this paper, we show that exposure of (3×3) 6H-SiC $(0001)_{Si}$ surfaces to atomic hydrogen from a remote rf plasma source results in complete removal of all Si-Si bonded silicon from the surface leaving a (1×1) surface. In turn, TPD showed weak H_2 desorption in the range of 400-600°C where desorption from silicon atoms would be expected based on analogy to (111) Si surfaces [13-19]. A corresponding rise in H_2 desorption was observed at higher temperatures where H_2 desorption from carbon sites would be expected based on analogy to (111) diamond surfaces [32, 34] and which in turn suggests C-H termination of the SiC surface. This was supported by the observation of some C-C bonding after thermal desorption of the rf plasma treated SiC surface at T > 1000°C. Similar to results previously reported by other researchers, we also observed removal of silicon from single crystal (3×3) 6H-SiC $(0001)_{Si}$ SiC surfaces using smaller fluxes of atomic hydrogen generated from a hot rhenium filament. In this case, complete removal of all Si-Si bonded silicon was not observed, but TPD was able to detect H_2 desorption in the range of 300-500°C indicative of Si-H desorption. However, the hydrogen desorption in this temperature range was broad and irregular resembling desorption from (2×1) B/Si (001) surfaces [78].

II. Experimental Procedure

All experiments described below were conducted using a unique ultra high vacuum (UHV) configuration which integrates several completely independent UHV surface preparation, thin film growth and surface analysis systems via a 36 ft. long transfer line having a base pressure of 9 10^{-10} Torr (see Refs. 76 and 79 for details of the transfer line, and many of the associated systems). The experiments described in this paper employed the SiC atomic layer epitaxy (ALE)/temperature programmed desorption (TPD), Auger electron spectroscopy (AES), low energy electron diffraction (LEED), x-ray photoelectron spectroscopy (XPS), and remote H plasma systems. A brief description of these systems is provided below.

The SiC ALE system consisted of a UHV chamber with a base pressure of 3×10^{-10} Torr and was equipped with a residual gas analyzer (RGA) and a variety of gas dosers. For TPD experiments, the RGA (a 0-200 amu quadrapole gas analyzer from Hiden Analytical Ltd.) was housed in a separate differentially pumped cylindrical chamber (similar in design to that of Smentkowski and Yates [80]). The RGA chamber had a 0.5 cm diameter orifice at the head of the RGA for TPD experiments and an approximately 50 cm^2 "sunroof" which could be opened to allow monitoring of residual gases in the system. The sample heating stage for the TPD experiments consisted of a wound tungsten heating filament positioned close to the back of the sample and mounted on a boron nitride disk [79]. A W/6%Re-W/26%Re thermocouple was employed to measure the temperature of the backside of the wafer. Heating profiles to 1100°C

were easily obtained using a programmable microprocessor and 20 amp SCR power supply. Actual surface/sample temperatures (i.e. those reported herein) were measured using an infra-red pyrometer with a spectral response of 0.8 to 1.1 μm and a emissivity setting of 0.5. The estimated experimental accuracy for the latter temperatures was estimated to be ± 25°C.

Low fluxes of atomic hydrogen were generated in the ALE system using a hot filament fabricated from 0.25 mm diameter rhenium wire. Temperatures >1700°C as measured by the previously mentioned optical pyrometer were used to generate the atomic hydrogen. The rhenium filament was positioned approximately 3 1/2" away from the SiC wafer. No attempts were made to try and accurately measure the atomic H flux at the SiC surface, and exposures were quoted in units of Langmuirs (10^{-6} Torr sec.). All hot filament atomic H exposures were conducted without heating of the SiC by the sample heater (i.e. room temperature). Any heating of the SiC surface by the hot filament is felt to be minimal and at most could have raised the surface temperature by 100°C.

The XPS experiments were performed in a stainless steel UHV chamber (base pressure = 2×10^{-10} Torr) equipped with a dual anode (Mg/Al) x-ray source and a 100 mm hemispherical electron energy analyzer (VG CLAM II). All XPS spectra reported herein were obtained using Al Kα radiation (hν = 1486.6 eV) at 12 kV and 20 mA emission current. XPS analysis typically required less than 1 hour during which time the pressure never increased above 9×10^{-10} Torr. Calibration of the binding energy scale for all scans was achieved by periodically taking scans of the Au $4f_{7/2}$ and Cu $2p_{3/2}$ peaks from standards and correcting for the discrepancies in the measured and known values of these two peaks (83.98 and 932.67 eV, respectively) [81]. Curve fitting of most data was performed using the software package GRAMS 386. A combination Gaussian-Lorentzian curve shape with a linear background was found to best represent the data. The Auger electron spectrometer and the low energy electron diffraction optics were mounted on a six way cross off the transfer line and pumped through the transfer line. In the AES analysis, a 3 keV, 1mA beam was used. Each Auger electron spectrum was collected in the undifferentiated mode and numerically differentiated. In LEED an 80 eV, 1mA beam was used.

The plasma system consisted of an all metal seal stainless steel vacuum chamber pumped by a 330 l/s turbomolecular pump. The base pressure of this system was 4×10^{-9} Torr and was limited by the double o-ring sealed quartz tube attached to the top of the system where the rf discharge was produced. The process gases flowed through this quartz tube and an inductively coupled plasma was generated using an rf power supply (13.56 MHz) and rf matching network attached to a copper coil wrapped around the quartz tube. The sample was located 40 cm down from the center of the rf coil. An inline Nanochem purifier and filter was used for point of use purification of hydrogen. Sample heating in the plasma system was conducted using a sample heater similar in design to the one previously described in the ALE system. Depending on the

chamber pressure and rf power, the plasma could be maintained in the quartz tube or extended down toward the sample region. For the experiments described in this study, an rf power of 20 W and a chamber pressure of 10-15 mTorr was used which confines the plasma to the quartz tube (i.e. a remote plasma). The plasma system was also equipped with a differentially pumped 0-100 amu RGA which allowed direct analysis of the purity of the process gases. RGA analysis of the hydrogen (99.999% purity) used in these experiments after *in situ* purification revealed that the impurity level of these gases were below the baseline of the system (<1ppm).

The n-type ($N_D=10^{18}/cm^3$), 1" diameter, off axis (4° toward {11-20}) $(0001)_{Si}$ 6H-SiC wafers used in this research were supplied by Cree Research with an ≈ 1 μm n-type ($N_D=10^{17}/cm^3$) 6H epilayer and a 1000Å thermally grown oxide. The thermal oxide was removed by a 10 min. dip in 10:1 HF. The unpolished back side of each wafer was subsequently coated via RF sputtering with tungsten to increase the heating efficiency of the SiC, as the latter is partially transparent to the infrared radiation emitted from the tungsten filament heater. After coating the backside of the SiC wafer with tungsten, the SiC wafers were ultrasonically rinsed in trichloroethylene, acetone and methanol each for 5-10 min. and then exposed to the vapor from a 10:1 buffered HF solution for 10 min. The wafers were then mounted to a 1" diameter ring shaped Mo sample holder using Ta wire and inserted into the transfer line load lock for experimentation. The SiC wafer was then loaded into the SiC ALE system and annealed in 10^{-6} Torr SiH_4 for 15 min. at 1050°C. This produced an oxygen free (3×3) reconstructed surface [76]. For comparison purposes, Si (111) wafers were also examined in this study. In this case, n-type (0.8-1.2 Ω cm) Si (111) wafers were cleaned by dipping in 10:1 HF to remove the thermal oxide and then annealed in the ALE system at 950°C. This produced an oxygen free (7×7) reconstructed surface.

III. Results

Interaction of rf Atomic H with (3×3) Vicinal $(0001)_{Si}$ 6H-SiC Surfaces. Figure 1a shows an AES spectrum obtained from a $(0001)_{Si}$ 6H-SiC wafer after annealing in SiH_4 to produce the (3×3) reconstructed SiC surface. As illustrated, the treatment removes oxygen from the SiC surface to levels below the detection limit of AES and produces a silicon rich surface. Accounting for the 2:1 difference in sensitivity between Si and C in AES [47], the Si/C peak to peak height (pph) ratio for the 3×3 surface shown here was 1.35. Figure 2a shows an XPS spectrum of the Si 2p core level obtained from the same surface. As displayed, two peaks at 99.5 and 101.5 eV were detected by XPS and which were indicative of Si-Si and Si-C bonding respectively. This figure indicates the > 1 Si/C pph ratio in AES for the (3×3) 6H-SiC surface is primarily due to excess silicon deposited on the surface. In previous studies, it has been

shown that the (3×3) reconstruction corresponds to an incomplete bilayer coverage of silicon on top of the SiC surface [67,68,76].

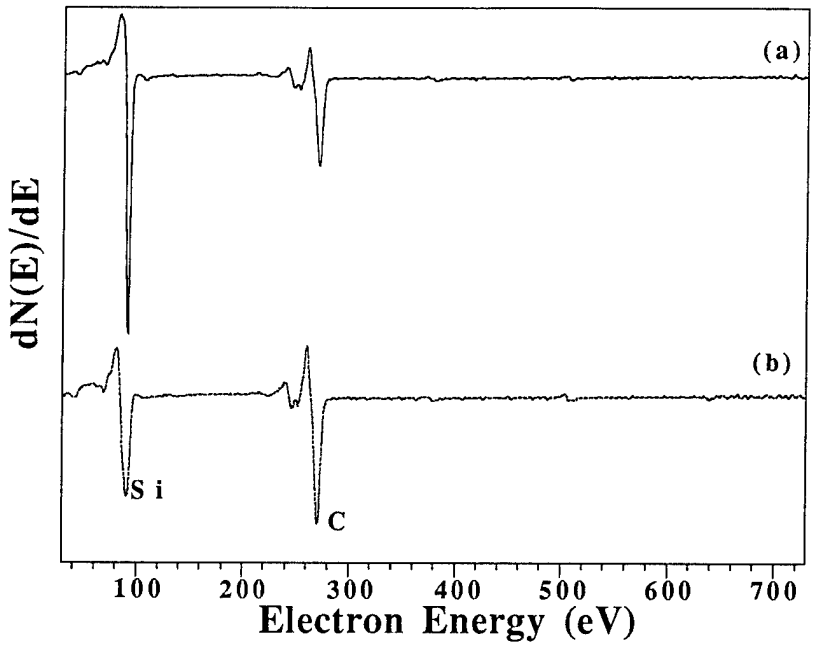

Figure 1. AES of (3×3) reconstructed $(0001)_{Si}$ 6H-SiC (a) before remote H plasma, and (b) after remote H plasma (1 min., 20 W, 15 mTorr, and 450°C)

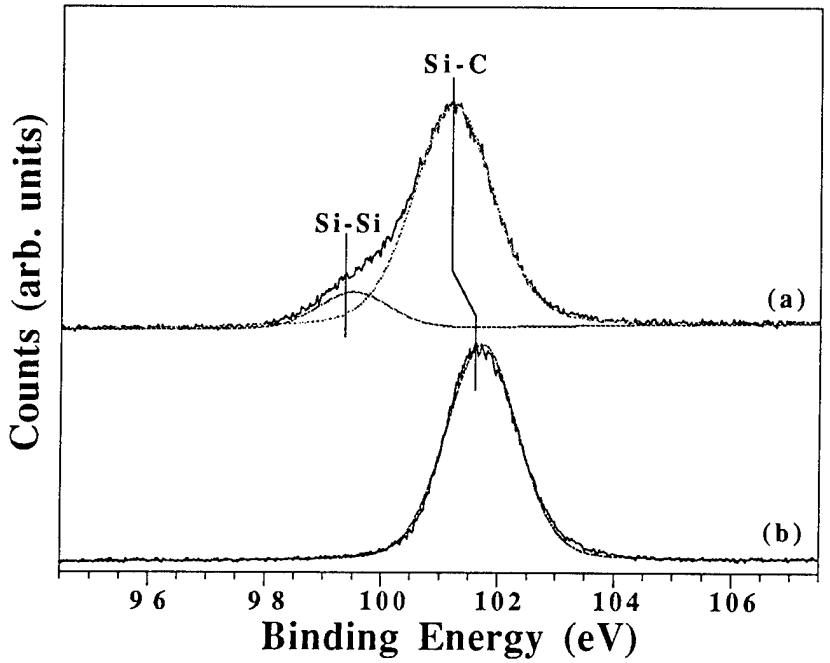

Figure 2. XPS of the Si 2p core level from (3×3) reconstructed $(0001)_{Si}$ 6H-SiC (a) before remote H plasma, and (b) after remote H plasma (1 min., 20 W, 15 mTorr, and 450°C)

Figure 1b shows an AES spectrum obtained from the (3×3) 6H-SiC $(0001)_{Si}$ wafer after a 1 min., 450°C remote rf plasma treatment (20W, 15 mTorr). As can be seen, the intensity of the Si LVV transition is greatly reduced by the rf plasma exposure and the corresponding Si/C pph ratio is reduced to 0.4. Correspondingly, a reduction/elimination of the Si-Si bonding peak in the Si 2p XPS spectrum was also observed (see Fig. 2b). (Note: the shift in energy of the Si 2p anc C 1s core levels with H plasma processing is related to band bending effects discussed in a separate paper [77]). Additionally, the LEED pattern from this surface was observed to switch from (3×3) to (1×1). The (1×1) pattern was composed of broad dots suggestive of increased surface disorder. This etching phenomena was observed to occur throughout the temperature range investigated (25-800°C). At this point, we also note that the pph Si/C ratio obtained in AES here was very similar to the value of 0.47 obtained by Allendorf *et al.* [47] from polycrystalline 3C-SiC films exposed to thermally generated atomic H.

As hydrogen can not be detected by either AES or XPS, TPD was used to confirm that hydrogen adsorbed or desorbed from the SiC surface. Figure 3 shows a TPD spectrum obtained from the 450°C rf plasma treated SiC surface. In our case, we were only able to observe a weak desorption feature centered around 600°C. Beyond this feature, the intensity of the H_2 signal was observed to gradually increase to the endpoint of our temperature data acquisition hardware which is 950°C. This gradual hydrogen desorption at higher temperatures could be related to the hydrogen desorption observed from 450-950°C by Allendorf *et al.* [47]. However, it could also be due to desorption of subsurface hydrogen or outgassing from our heater. Allendorf *et al.* [47] have previously noted desorption/outgassing of subsurface hydrogen at 1000°C from their polycrystalline 3C-SiC films due to residual hydrogen trapped in the SiC during CVD growth of the SiC film. However in their case, the outgassing feature was observed to be quite abrupt and intense whereas we observed a gradual rise in the H_2 signal. Additionally, we typically observe higher levels of outgassing of subsurface hydrogen from rf plasma treated silicon wafers at much lower temperatures (data not shown). This could however be related to the observation of Keroak and Terreault [65] that implanted deuterium desorbs from silicon at relatively lower temperatures than SiC (1200 vs. 2700°C).

To test outgassing of our heater as a source of hydrogen in TPD experiments on plasma treated SiC, we acquired a TPD spectrum of the heater just prior to the SiC TPD experiments (see Fig. 4a). As can be seen, an essentially featureless spectra was obtained with the detected H_2 signal being two orders of magnitude lower than that from the plasma treated SiC. To test outgassing of the moly sample holder, we additionally performed TPD on a 1" diameter molybdenum plate exposed to the same plasma conditions as the SiC wafer (see Fig. 4b). In this case, we observed a large and broad desorption spectrum centered at ≈ 550°C which is typical for surface and subsurface desorption.

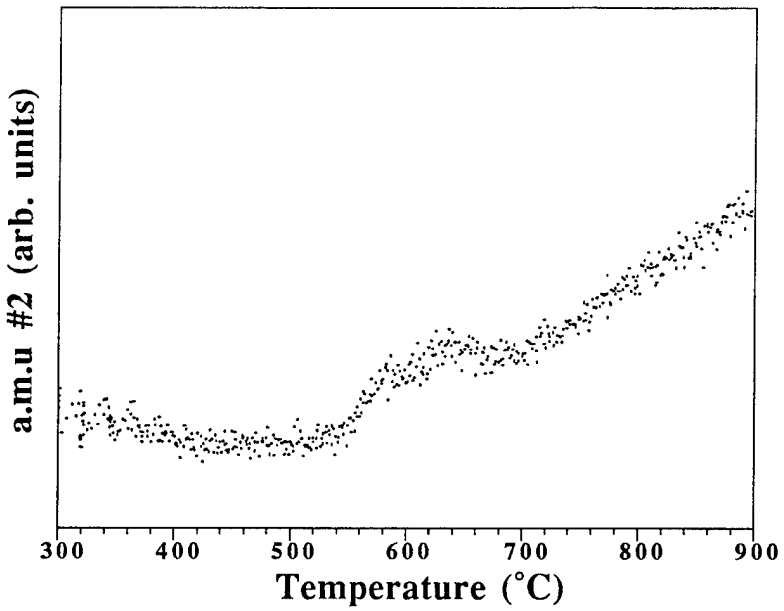

Figure 3. TPD of (1×1) 6H-SiC $(0001)_{Si}$ after remote H plasma exposure (1 min., 20 W, 15 mTorr, and 450°C), (ß = 1°C/sec.).

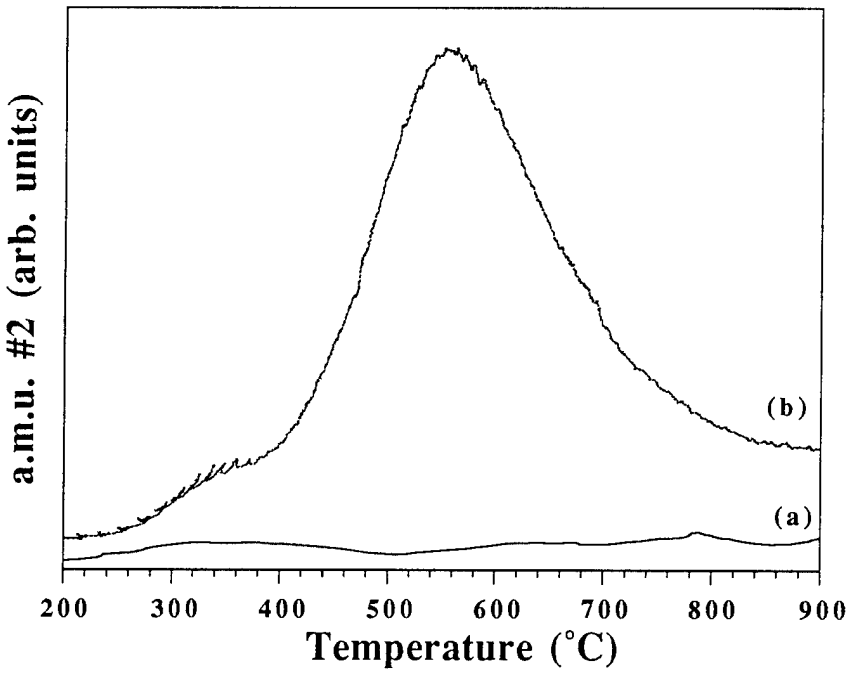

Figure 4. TPD of (a) sample heating stage after outgassing, and (b) molybdenum plate after remote H plasma exposure (1 min., 20 W, 15 mTorr, and 450°C), (ß=1°C/sec.).

Finally, XPS of the C 1s core level before and after TPD revealed the presence of a second C 1s peak after TPD (see Fig. 5). However after TPD, the SiC surface still displayed a (1×1) LEED pattern. Before TPD, the XPS showed only one C 1s peak. After TPD, a second peak at higher binding energy appeared and which is indicative of some C-C bonding at the surface. In the TPD experiments, the SiC wafer dwells at the maximum temperature (≈1000°C) for less than a minute. In our experience, the time at this temperature is not sufficiently long enough to result in the volatilization of a enough silicon to produce this much C-C bonding at the surface alone. Therefore, the appearance of some C-C bonding must be related to the loss of hydrogen from the SiC surface.

Interaction of Thermal Atomic H with (3×3) vicinal $(0001)_{Si}$ 6H-SiC Surfaces. In order to separate out subsurface hydrogen outgassing and other plasma related induced effects, atomic H generated via cracking H_2 over a hot rhenium filament was also used as a source of atomic hydrogen. For comparison purposes, TPD spectra were first acquired from (7×7) Si (111) surfaces exposed to atomic hydrogen generated by the hot filament. In these experiments, it was observed that the surface switched to (1×1) after the atomic H exposure. Figure 6 shows a TPD spectrum acquired from the hydrogen terminated (1×1) Si (111) surface. As can be seen, a sharp desorption peak centered at ≈ 475°C typical of monohydride ($ß_1$) desorption from silicon was observed [13,15-18]. The shoulder at lower energies was assigned to dihydride

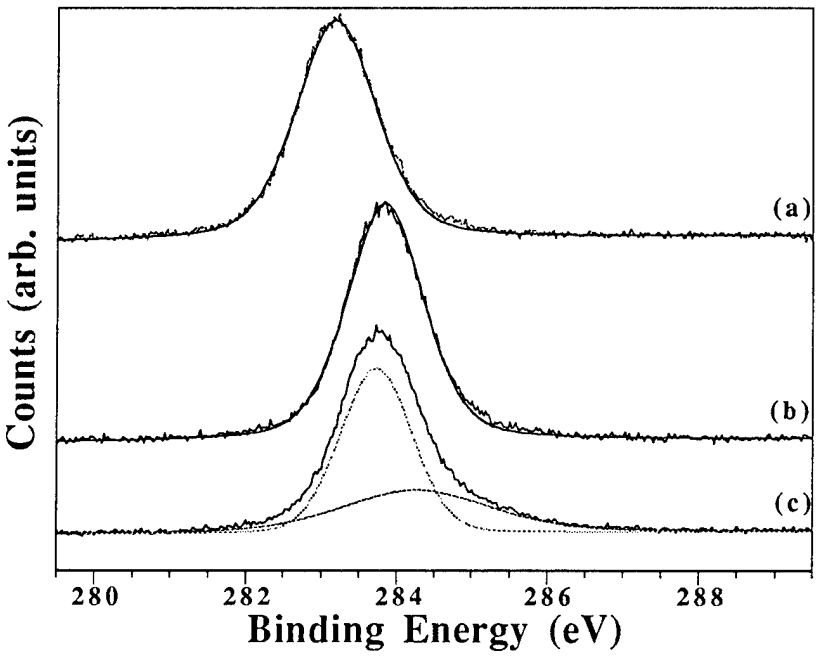

Figure 5. XPS of the C1s core level from $(0001)_{Si}$ 6H-SiC (a) before remote H plasma, (b) after remote H plasma (1 min., 20 W, 15 mTorr, and 450°C), and (c) after annealing at 1000°C.

and trihydride ($ß_{2,3}$) desorption from silicon [13,15-18]. The ability to detect these features demonstrates the ability of the hot filament to produce atomic hydrogen as well as validates our TPD apparatus.

Figure 7 shows an AES spectrum of a (3×3) 6H-SiC $(0001)_{Si}$ surface before and after exposure to atomic H (2000 Langmiur H_2) from the hot rhenium filament. In this case, the hot filament H exposure was observed to still maintain a Si/C ratio of > 1 but the ratio did decrease from 1.35 to 0.9 and the LEED pattern was observed to switch from (3×3) to (1×1) (however, in this case the LEED pattern displayed sharp dots). This observation was supported by a similar reduction in the intensity of the Si-Si Si 2p peak in XPS. Unlike the (111) Si surface however, a sharp desorption feature was not observed from the SiC surface exposed to atomic H (see Fig. 8) with only broad H_2 desorption in the range of 350-650°C being detected. In this case, the SiC TPD spectra more closely resembled the TPD spectra of Kim *et al.* [78] obtained from (2×1) B/Si (001) surfaces. Additionally, XPS did not detect any C-C bonding at the SiC surface after TPD of the SiC surfaces treated with atomic H from the hot filament.

As a final check, TPD spectra were also acquired from chemically vapor/silane cleaned (3×3) SiC surfaces which had been cooled in the silane to ≈ 300°C (see Fig. 9). The samples were cooled in SiH_4 to 300°C to hopefully maintain some hydrogen termination of the SiC surface without preferentially losing silicon from the surface. In this case, more pronounced hydrogen desorption at 475-525°C was observed and which was more comparable

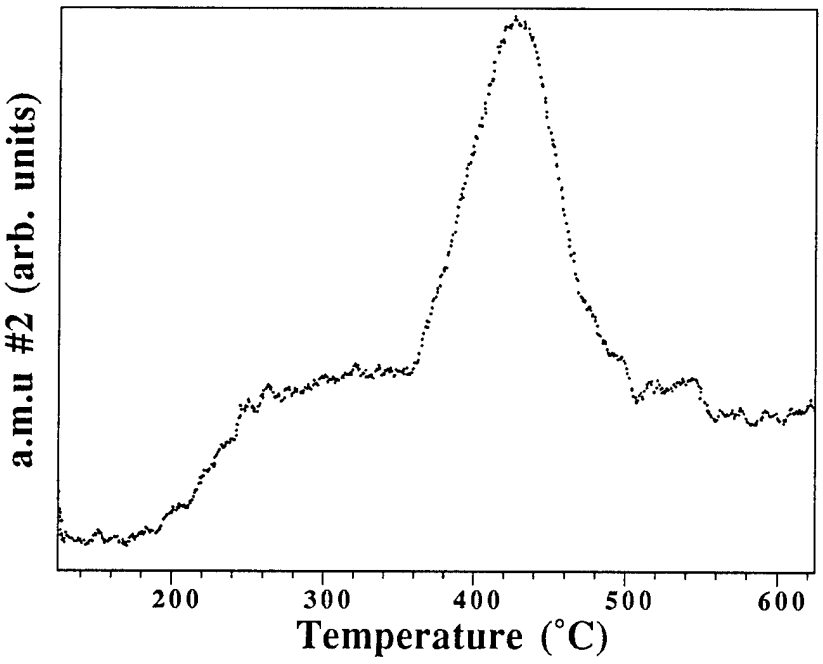

Figure 6. TPD of Si (111) after room temperature exposure to 2000£ H_2 with rhenium filament at > 1700°C (ß=1°C/sec.)

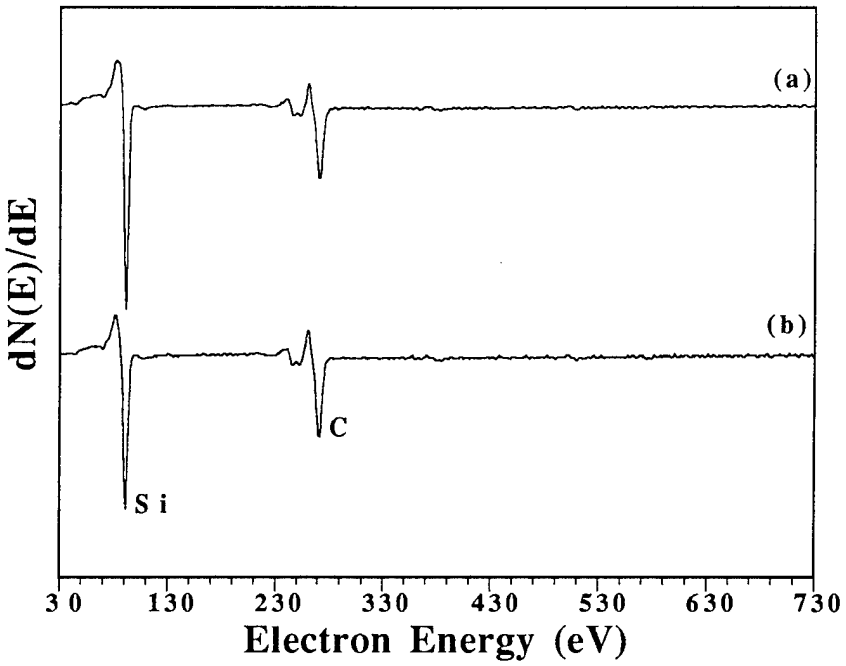

Figure 7. AES of (3×3) 6H-SiC $(0001)_{Si}$ (a) before atomic H exposure and (b) after room temperature exposure to 2000£ H_2 with hot filament at > 1700°C.

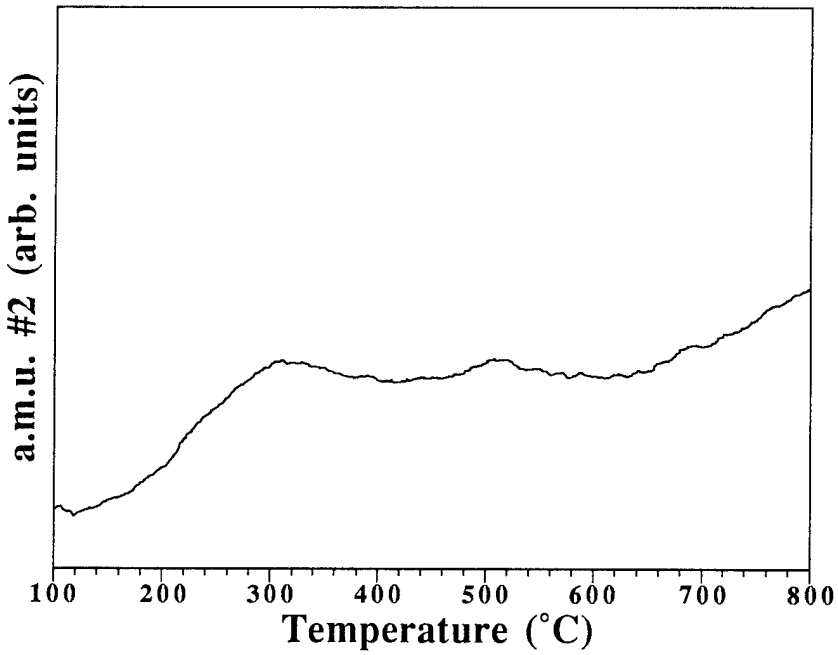

Figure 8. TPD of $(0001)_{Si}$ 6H-SiC after room temperature exposure to 2000£ H_2 with rhenium filament at > 1700°C (ß=1°C/sec.)

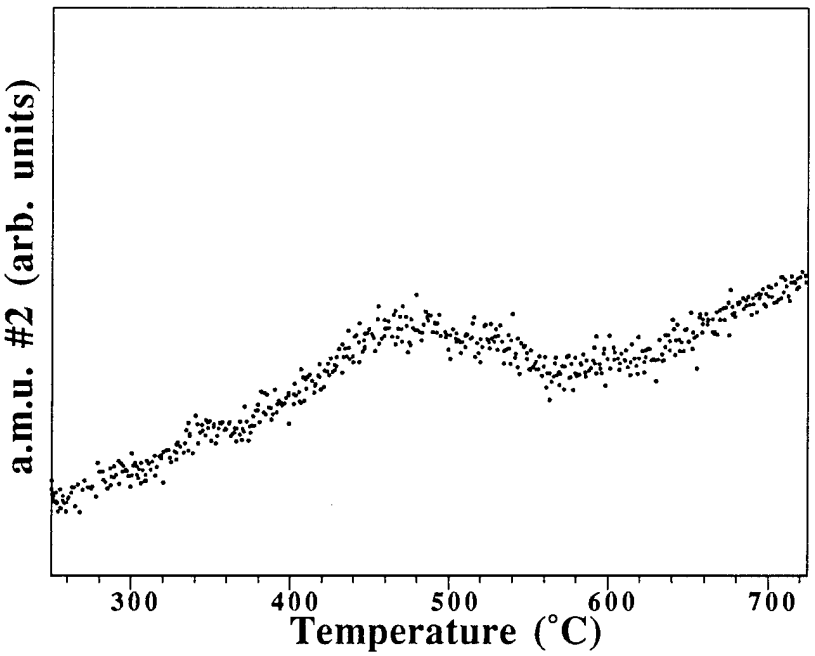

Figure 9. TPD of (3×3) 6H-SiC $(0001)_{Si}$ after cooling to 300°C in 10^{-6} Torr SiH_4 (ß=1°C/sec.)

to hydrogen desorption from the Si (111) TPD spectra. However, the intensity of this hydrogen desorption feature was not nearly intense or sharp as that observed from the Si (111) wafer. This could be related, though, to the inability of the silane flux to maintain a hydrogen terminated surface at low temperatures.

IV. Discussion

In order to gain a better understanding of the observed etching of SiC surfaces presented above, the authors feel that it is necessary to first separately consider the etching of the two elemental components of SiC (i.e. silicon and diamond). Previous studies have reported etching of silicon [14,24,28], diamond [32,34,37,39], and amorphous silicon carbon alloys [82] by atomic hydrogen produced either via plasma excitation or thermal decomposition. In the case of silicon, atomic hydrogen etching has been associated with the formation of di and trihydrides (SiH_2(a) and SiH_3(a)) on the silicon surface. These species have been shown to be the precursors for the final etch product, silane (SiH_4(g)) [14,24]. However, SiH_2(a) and SiH_3(a) species were only observed to form at low temperatures (0-200°C) where hydrogen desorption is negligible. At higher temperatures (>350°C) were hydrogen desorption from di and trihydride sites is more appreciable, the silicon surface was observed to be terminated by mostly monohydrides (SiH(a)) and the yield of etch products such as SiH_4(g) and Si_2H_2(g) decreased. Correspondingly, studies on H plasma cleaning of silicon have observed

etching/roughening of silicon surfaces at temperatures < 450°C and no surface roughening at temperatures > 450°C [28].

In the case of diamond, etch products such as CH_x and C_2H_x have not been observed from (001) or (111) single crystal diamond surfaces exposed to atomic H. TPD experiments on single crystal (001) [32,34] and (111) [38] diamond surfaces have only shown recombinative desorption of hydrogen at ≈ 1000°C. Etch precursors such as CH_x or C_2H_x at ≈ 425°C have only been observed via TPD from (001) and (111) oriented polycrystalline CVD diamond films exposed to atomic H [39]. However, Kuttel *et al.* [37] clearly have observed etching of (001) and (111) single crystal diamond surfaces at temperatures up to 870°C in a microwave H plasma via a measured decrease in RMS surface roughness from 7 nm to 1 nm after plasma processing. The long etch time (17 hr.) required by Kuttel to produce these results indicates that the formation of CH_x species on diamond surfaces by atomic H is perhaps slow or inefficient.

The simple observation that H plasma etching of diamond surfaces occurs at higher temperatures than that observed in the case of silicon suggests that perhaps the atomic H etch rates for silicon and carbon in SiC will be different. In fact, this has already been observed for amorphous SiC films. Using XPS and glancing incidence XRD, Kalomiros *et al.* [82] have shown preferential etching of silicon from an a-SiC surface and the formation of a polycrystalline hydrogenated carbon layer by a rf plasma process at 230°C. This behavior is exactly what should be predicted based on analogy to the observed etching characteristics of diamond and silicon. This behavior is also consistent with our observation of the selective removal of excess silicon from (3×3) $(0001)_{Si}$ 6H-SiC surfaces by atomic H generated both by plasma excitation and thermal decomposition.

A second observation to be made based on analogy to silicon and diamond is that atomic H etching of surfaces generally occurs at low temperatures where hydrogen desorption is low and a fully hydrogenated surface can be maintained. Therefore, in order to better understand the etching characteristics of SiC surfaces in atomic H, we have attempted to estimate the hydrogen surface coverage of silicon carbide surfaces in an atomic H flux. To do this, we have used a simple model in which we consider hydrogen adsorption and desorption from silicon and carbon sites separately. The adsorption/desorption processes at silicon and carbon sites are modeled using published data for the kinetics of these processes on (001) silicon [23,31] and (001) diamond surfaces respectively [32,34]. Although the experimental data presented in this study is for (111)/(0001) oriented surfaces, the choice to use kinetic parameters from (001) orientations is primarily for sake of consistency as kinetic parameters for hydrogen desorption from (111) diamond surfaces are not available. The values for E_{des} and ν used in these calculations are presented in Table I.

Table I. Kinetic Parameters used to Model Hydrogen Adsorption/Desorption from Si and C Sites on SiC Surfaces. (Note: the data shown below are for first order processes).

	Si		C	
	$ß_1$	$ß_{2,3}$	Hamza [32]	Thomas [34]
E_{des} (kcal/mol)	47 [23] 25 [31]	37	72.7	
ν (#/sec)	8×10^{11}	10^7	3×10^5	10^{13}

For the carbon sites, hydrogen desorption was modeled using the kinetic parameters determined for hydrogen desorption from (001) diamond surfaces by both Hamza *et al.* [32] and Thomas *et al.* [34]. This is primarily a result of the extremely low value of 37 kcal/mol for E_{des} reported by Hamza *et al.* [32] which is lower than that reported for silicon. This value for E_{des} is extremely surprising given the simple fact that hydrogen desorption from diamond surfaces occurs at temperatures 500°C higher than on silicon. Therefore, the data of Thomas *et al.* [34] was used as well since in this case E_{des} = 72.7 kcal/mol which is higher than most values reported for H_2 E_{des} from silicon surfaces. Additionally, Allendorf *et al.* [47] have also reported E_{des} = 72 kcal/mol and $\nu = 10^{13}$/sec for hydrogen desorption from polycrystalline SiC surfaces.

To estimate the SiC hydrogen surface coverage, we employ the method of Schulberg *et al.* [94] in which we assume a steady state equilibrium between the incoming flux of atomic H and surface desorption of H_2. Desorption kinetics are typically described by the general Polyani-Wigner rate expression [31]:

$$\text{desorption rate} = -d\emptyset/dt = \nu^n \exp(-E_{des}/RT) \qquad (1)$$

where:

n = the reaction order

$\emptyset$ = the adsorbate surface coverage

ν = the pre-exponential factor, $n_o = 10^{28}/cm^2$ sec,

$\nu_1 = 10^{13}$/sec, $n_2 = 10^{-2}$ cm^2/sec

E_{des} = the activation energy for desorption

In steady conditions, the flux of adsorbates leaving the surface via desorption will be equal to the incoming flux of adsorbate times the adsorbate sticking coefficient. The sticking coefficient is described by:

$$S = S_o(1 - \emptyset/\emptyset_{max})^n \qquad (2)$$

where

S = Sticking Probability

S_o = Initial Sticking Probability (i.e. S at $\emptyset = 0$)

$\emptyset_{max}$ = Maximum Surface Coverage

The combination of Eqs. 1 and 2 allows the determination of the steady state surface coverage of the adsorbate [94]. Based on this model and the desorption kinetic data tabulated above, we have estimated the surface coverage of hydrogen on silicon and carbon sites both as a function of temperature and flux. The results are presented in Figs. 10-13 and are based on the assumption of a unity initial sticking coefficient (i.e. $S_o = 1$).

Figures 10 and 11 show the estimated monohydride and di/trihydride surface coverages for silicon sites as a function of temperature and flux (ML/sec). Figure 10 indicates that in fluxes typical of low pressure hydrogen plasma processes, all silicon sites should be saturated with hydrogen up to temperatures of ≈ 800°C. However, Fig. 11 indicates that the concentration of di/trihydrides should start to decrease around 500-600°C. Although the temperature range is slightly higher, this is clearly consistent with the previously reported etching behavior of silicon in a remote H plasma. Accordingly, etching of silicon in SiC should stop or decrease at temperatures above ≈ 600°C. However, as shown in Figs. 12 and 13, carbon sites on SiC surfaces should remain saturated with hydrogen up to temperatures of 1000-1100°C indicating that etching of carbon in SiC could continue up to temperatures these very same temperatures.

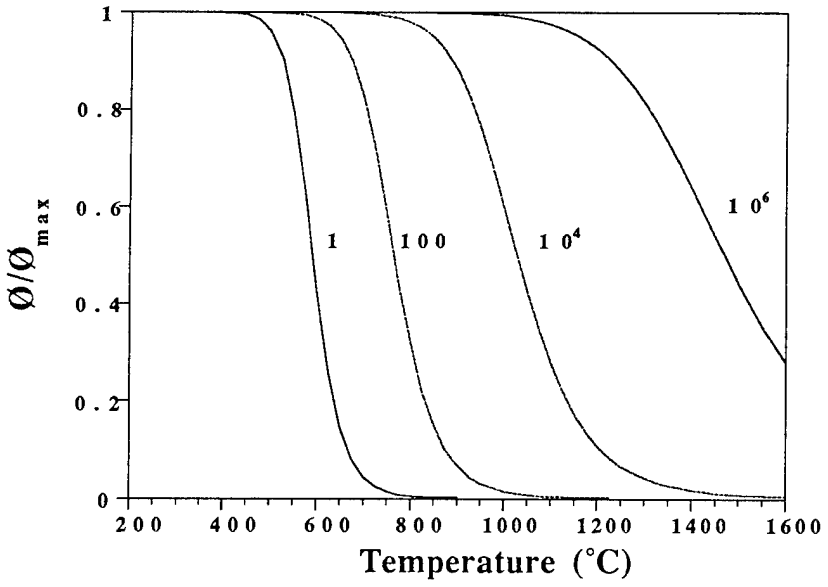

Figure 10. Mono-hydride surface coverage on silicon sites of SiC.

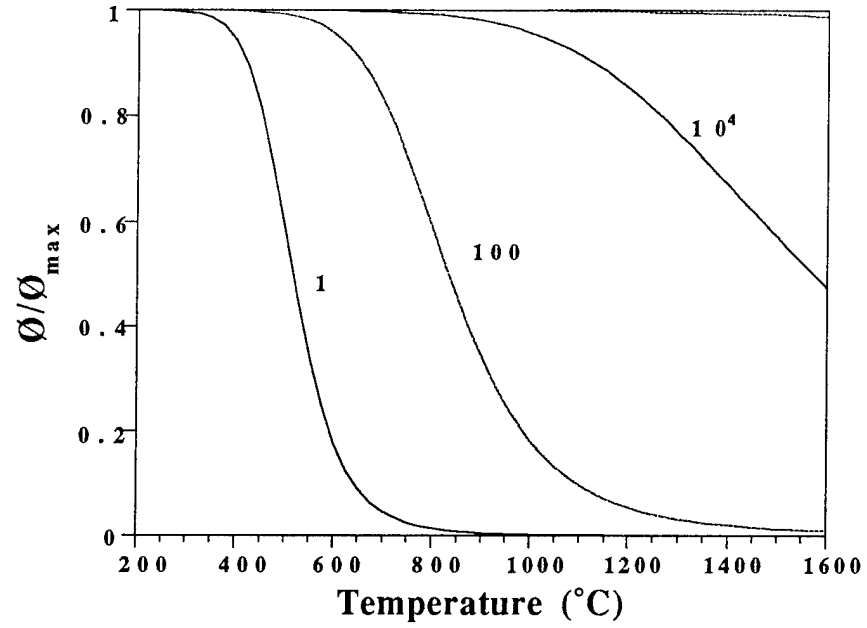

Figure 11. Di-hydride surface coverage on silicon sites of SiC.

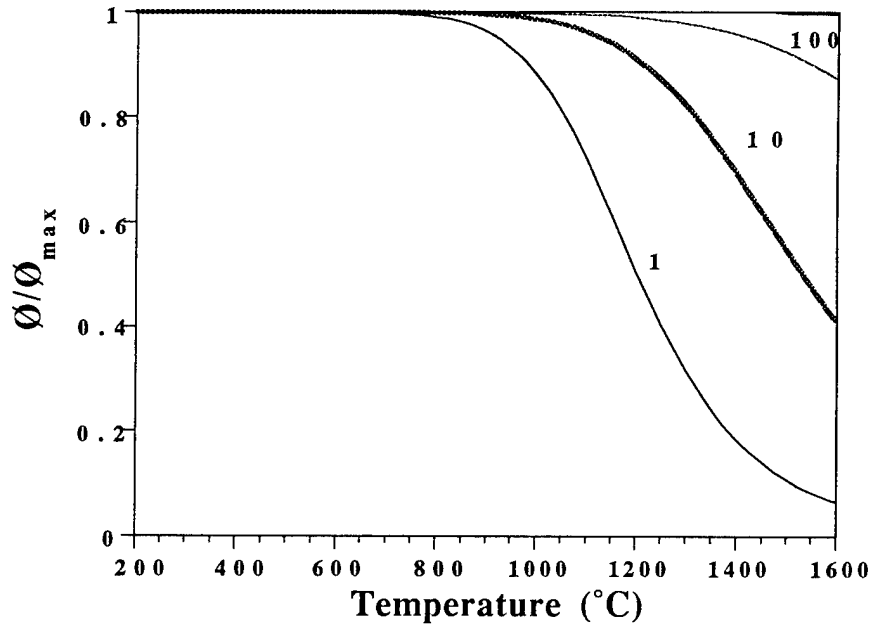

Figure 12. Hydrogen surface coverage on carbon sites of SiC based on kinetic data of Hamza [32].

We also note the significant difference in predicted concentration of occupied carbon sites based on the data of Hamza *et al.* [32] and Thomas *et al.* [34]. Based on the data of Hamza *et al.* [32], carbon sites would be expected to be saturated with hydrogen up to 1200°C in a 100 ML/sec H flux. However, the data Thomas *et al.* would predict that at least of half of these sites would be empty under the same conditions.

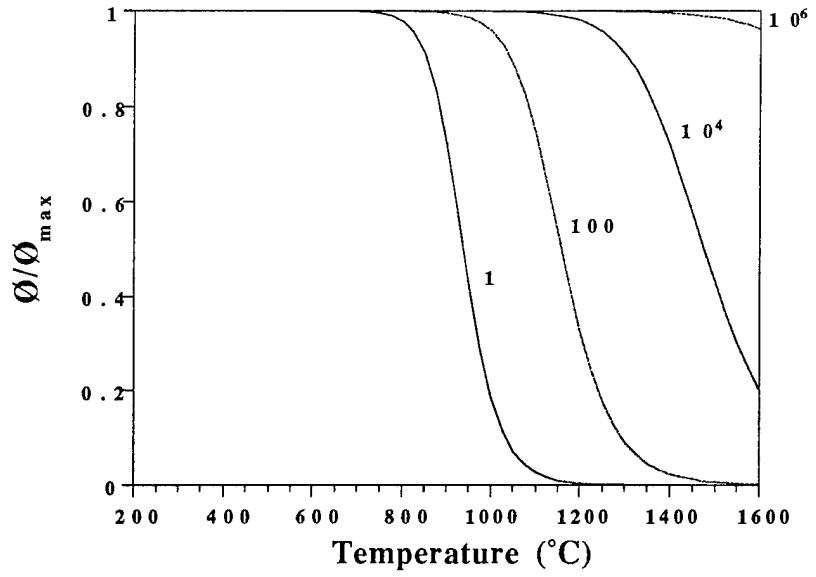

Figure 13. Hydrogen surface coverage on carbon sites of SiC based on kinetic data of Thomas *et al.* [34].

Based on analogy to silicon and Figs. 10-13, one would expect etching of SiC in atomic H at temperatures < 1000°C and no etching at temperatures ≈ > 1000°C. In reality, SiC is probably etched by atomic H at all temperatures. However, the etch rate probably exhibits some temperature dependence. At low temperatures (i.e. RT-500°C), the etch rate is probably low due to limited thermal activation and perhaps surface mobility. As the temperature is increased into the range of 500-1000°C, the etch rate should decrease due to significant desorption of hydrogen through silicon sites and the reduction of etch precursors such as SiH_3(a). However, the etch rate in this temperature range will probably still be measurable due to limited desorption from carbon sites and hence the ability to form CH_x etch products. At temperatures > 1000°C, the etch rate should decrease due to increased desorption of hydrogen from both carbon and silicon sites but may eventually increases due to increased thermal activation and possible volatilization of silicon at temperatures >1500°C. This type of etch rate dependence has been partially observed by Kim and Olander [48] in their modulated molecular beam mass spectrometry studies. In these studies, they observed SiH_4, CH_4, and C_2H_2 etch products from polycrystalline 3C-SiC films during atomic H exposure over the temperature range of RT-800°C. However, the yield of SiH_4 from SiC was observed to initially increase with temperature and then start to decrease at ≈ 500°C. The yield of CH_4, however, was observed to gradually increase over the entire temperature range investigated (0-800°C). Though Kim and Olander [48] explain the decrease in SiH_4 production to depletion of silicon from the surface, their results are also clearly consistent with our explanation based on enhanced hydrogen desorption from silicon sites. However, our inability to avoid selective

removal of silicon from the (3×3) $(0001)_{Si}$ 6H-SiC surface in the rf H plasma over the temperature range of 0-800°C is also consistent with the results of Kim and Olander [48].

In the higher temperature range (1000-1700°C), it has been previously noted that the etch rate of SiC in molecular hydrogen (i.e. H_2) increases with increasing temperature. In this case, we feel that the actual etching of SiC is due to atomic H produced by thermal decomposition of molecular H_2. Figure 14 shows the predicted percent dissociation of molecular hydrogen into atomic hydrogen based on thermodynamic calculations (note figure produced by HSC program). As can be seen, significant production of atomic H is only predicted to occur at temperatures of 1500-1700°C. So these higher temperatures for molecular H_2 etching are at least to some extent probably necessary to produce a significant concentration of atomic hydrogen. The higher temperatures probably also assist in the volatilization of silicon from the surface as well as increasing the surface mobility.

At this point, it is worth considering some of the potential errors in this simplified model. First for this model to be valid, diffusion of hydrogen from carbon to silicon sites (and vice versa) must be minimal. For Si-Ge alloys this subject has sparked much debate. In this system, a lowering of T_{max} for monohydride ($ß_1$) desorption from silicon was observed with the addition of germanium to the surface [83,84]. This lowering of T_{max} has been argued to be due to weakening of the Si-H bond due to electronic matrix effects [83]. Others, however, have argued that the lowering of $ß_1$ T_{max} can be described by considering hydrogen diffusion from silicon sites to germanium sites where the activation energy for desorption is lower (E_{des} Si-H = 55 kcal/mol vs. Ge-H = 35 kcal/mol) [84,85]. This is reasonable for silicon surfaces where the activation energies for hydrogen diffusion on (100) and (111) surfaces have been

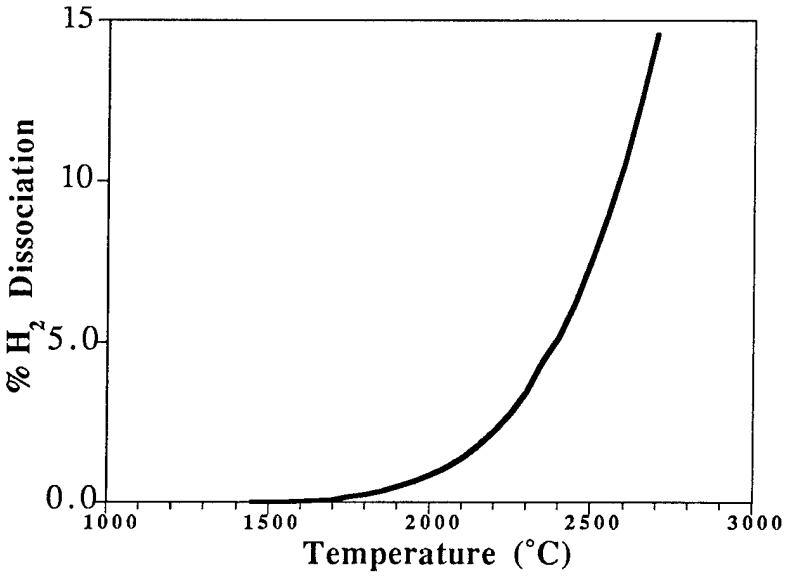

Figure 14. Percent dissociation of H_2 into H as function of temperature.

determined to be ≈ 30-41 kcal/mol [86,87] and 35 kcal/mole [88], respectively. Unfortunately for the case of SiC, activation energies for hydrogen surface diffusion have not been determined. However, activation energies for surface diffusion of Si and C atoms on SiC surfaces have been reported. Based on surface diffusion length measurements in CVD, Kimoto *et al.* [89,90] determined an activation energy of 82 kcal/mol for surface diffusion of Si or C atoms on $(0001)_{Si}$ 6H-SiC surfaces. These measured values are in agreement with the calculations of Takai *et al.* [91], which found activation barriers of 106-126 kcal/mol for carbon diffusion on (111) and (-111) 3C-SiC surfaces. As much lower activation energies for self diffusion of Si on Si (111) [92,93] and (001) [93] surfaces have been determined (18-35 and 6-25 kcal/mole respectively) it seems reasonable to expect the mobility of H atoms on SiC surfaces to be lower than on Si surfaces. Accordingly, H surface diffusion should be negligible in the temperature range studied here and should not affect our model.

Another possible source of error in our model is that T_{max} for hydrogen desorption from Si and C sites on SiC could be significantly different from that observed from silicon and diamond respectively. As previously mentioned, it has been suggested that the addition of Ge to Si lowers T_{max} for $ß_1$ H_2 desorption from Si sites due to a weakening of the Si-H bond by germanium [83]. It has additionally been observed that boron doping ($10^{19}/cm^3$) of Si also lowers T_{max} $ß_1$ whereas dosing Si (001) surfaces with diborane (B_2H_6) produces two $ß_1$ desorption features [78]. These effects have been explained based on varying electronic effects in which the Si-H bond is weakened by the more electronegative dopant or due to changes in the work function by the dopant or substitutional atom. Clearly, the addition of carbon to the silicon lattice (and vice versa) could have similar effects. The addition of carbon changes both the work function (and band gap) as well as creating a more polar bond with silicon to weaken any Si-H bonds at the surface. This line of reasoning could explain our inability to observe sharp desorption features from atomic H treated (3×3) $(0001)_{Si}$ 6H-SiC surfaces.

In the case of (3×3) SiC surfaces exposed and cooled in SiH_4 to 300°C, H_2 desorption at 475°C was observed and which was consistent with the observed H_2 desorption from Si (111) surfaces. This can be explained by the fact that for this surface all of the silicon atoms terminating the SiC surface have Si-Si backbonds as the (3×3) surface consists of a bilayer of silicon atoms. However, in the case of the hot filament atomic H treated (3×3) SiC surfaces, a broad range of H_2 desorption in the temperature range of 200-600°C was observed and which was similar in appearance to that observed from B_2H_6 treated Si (001) surfaces [78]. In this case, some of the Si bilayer has been removed via etching by atomic H and hence desorption occurs from Si atoms with Si-Si and Si-C backbonds (i.e. C-Si-H or Si-Si-H). For the silicon atoms with carbon backbonds, the Si-H bond is weakened as the underlying carbon atom is more electronegative and withdraws charge which the silicon atom would share with hydrogen. Accordingly, the weaker Si-H bonds translates into a lower E_{des}. This range of E_{des} is what

gives Fig. 8 its broad nature. However, we note that in the studies of Ascherl *et al.* [95] dosing silicon surfaces with trimethylsilane ($SiH(CH_3)_3$) did not result in any change in T_{max} for β_1.

In the case of the H plasma treated $(0001)_{Si}$ 6H-SiC surfaces, TPD showed a weak H_2 desorption feature at $\approx$ 625°C with a gradual increase in H_2 signal at higher temperatures. This feature is intermediate to what would be expected from carbon and silicon sites based on analogy to silicon or diamond surfaces. This feature could be related to H_2 desorption from CH_x sites, but is higher in temperature than previous reports of CH_x desorption from polycrystalline CVD diamond films [39]. This TPD spectrum, however, could be greatly effected surface roughening induced by the atomic H etching of the SiC surface. This could produce greatly affect E_{des}.

Setting aside our simple desorption model, etching of SiC by atomic hydrogen can also be predicted based on simple comparison of the Si-C, Si-H, and C-H bond energies which are 76.5, 70.8, and 98.8 kcal/mol respectively [97]. As can be seen, the C-H bond is actually stronger than the Si-C bond and energy can be gained by breaking a Si-C bond and forming a C-H bond. Although, the reaction between molecular hydrogen (H_2) and SiC to form Si-H and C-H bonds is not energetically favorable, i.e.

$$\begin{aligned} &\text{Si-C + H-H <=> Si-H + C-H} \qquad \text{(i)} \\ &\text{76.5+104 <===> 70.4 + 98.8} \\ &\text{179.7 <====> 169.2 kcal/mol} \end{aligned}$$

The reaction between pre dissociated atomic H and SiC is, i.e.

$$\begin{aligned} &\text{Si-C + 2H <=====> Si-H + C-H} \qquad \text{(ii)} \\ &\text{76.5 <====> 70.4 + 98.8} \end{aligned}$$

Thus for the $(0001)_{Si}$ 6H-SiC surface, it is more energetically favorable for atomic hydrogen to insert itself into a Si-C bond forming C-H bonds rather than simply terminating a Si dangling bond and forming a relatively weak Si-H bond. Thus, a C-H terminated SiC surface would be expected after atomic hydrogen exposure. This is in agreement with the < 1 Si/C pph ratio we and other have observed from SiC surfaces exposed to atomic H. This also agrees with our observation of the formation of some C-C bonding in XPS after TPD at 1000°C. At temperatures of 1000°C it would be expected that any hydrogen adsorbed on carbon would desorb leaving behind some C-C bonding. Additionally, we have previously noted that in HF wet chemical processing H termination of silicon atoms at $(0001)_{Si}$ 6H-SiC surfaces is highly unstable due to the polarity of the underlying Si-C bonds [96]. OH^- termination is instead favored due to the ability of the Si-OH bond to cancel the dipole produced by the Si-C bond below. For these same reasons, Si-H termination of $(0001)_{Si}$

6H-SiC surfaces in vacuum are equally unstable and hence there is an additional driving force for the H atom to insert itself into the Si-C bond. It is also worth mentioning that in the (3×3) structure there are actually a significant number of Si-Si bonds. We note that in this case, these bonds are compressed and distorted to values far from the their equilibrium value due to the differences in the lattice constants between Si and SiC (≈ 20 % [10,70-72]). As such, these bonds are probably more reactive with atomic hydrogen and it may be more energetically favorable to form SiH_x species rather than to remain in the distorted (3×3) structure.

Finally, the above results and discussion indicate that in H plasma cleaning of SiC, silicon should be added to the plasma chemistry in order to compensate for the selective removal of silicon from the SiC surface due to etching. The addition of silicon to the plasma (via SiH_4 or Si_2H_6) should also assist in the reduction of silicon oxides which are particularly difficult to remove in H plasmas. Lin *et al.* [51] have previously investigated cleaning of HF dipped SiC surfaces using a 1:1 H_2:He mixture in an ECR plasma source (650°C, 90 min., 5×10^{-4} Torr). In their case, they reported the removal of C-C, C-O, and C-F species from the SiC surface but were not successful in completely removing silicon oxides (Si-O) from the surface. The addition of silicon to the plasma chemistry therefore could assist in the removal of silicon oxides through chemical reduction and formation of more volatile sub oxides. Initial investigations in our lab using H_2/1%SiH_4 mixtures in plasma cleaning of HF dipped SiC surfaces have shown an enhanced removal of silicon oxides. However, deposition of silicon was a particular problem indicating that such a cleaning process requires delicately balancing the silicon deposition rate with its etching rate. This will require tight process control and perhaps only a very narrow processing window will be available.

V. Conclusion

In conclusion, we have shown that atomic hydrogen exposure selectively removes silicon from (3×3) 6H-SiC $(0001)_{Si}$ surfaces. Atomic hydrogen exposures reduces and removes the Si-Si bonding Si 2p XPS peak and converts the (3×3) LEED pattern to (1×1). Additional etching of the SiC surface was indicated by the reduction in the Si LVV/C KLL ratio in AES from 1.3 to 0.4 following exposure of (3×3) surfaces to a remote rf H plasma. TPD of atomic H treated (3×3) SiC surfaces showed weak hydrogen desorption in the range of 400-600°C where desorption from silicon atoms would be expected by analogy to (111) Si. However, the hydrogen desorption signal increased at higher temperatures where hydrogen desorption from carbon sites would be expected based on analogy to (111) diamond surfaces. C-H termination of the SiC surface was supported by the observation of some C-C bonding after thermal desorption of rf plasma treated SiC surface at T > 1000°C. Based on these observations, we conclude that atomic H processing of SiC surfaces selectively removes silicon from the surface and favors C-H termination.

VI. Acknowledgments

The authors would like to thank Cree Research, Inc. for supplying the 6H-SiC wafers. The research was supported by the Office of Naval Research under contract and through the Department of Education through an Electronic Materials/GAANN Fellowship.

VII. References

Examples of H_2 in Si Semiconductor Processing

1. S.S. Iyer, M. Arienzo, and E. de Fresart, Appl. Phys. Lett **57**, 893 (1990).
2. H.J. Stein, Appl. Phys. Lett. **32**, 379 (1978).
3. K.G. Drujif, J.M.M. de Nijs, E. van der Drift, E.H.A. Granneman, and P. Balk, Appl. Phys. Lett. **67**, 3162 (1995).
4. G.R. Srinivasan, J. Cryst. Growth **70**, 201 (1984).
5. H. Habuka, J. Tsunoda, M. Mayusumi, N. Tate, and M. Katayama, J. Electrochem. Soc. **142**, 3092 (1995).

H_2 in SiC Processing

6. N. Nordell, A. Schoner, and S.G. Andersson, J. Electrochem. Soc. **143**, 2910 (1996).
7. T. Kimoto, H. Nishino, W.S. Yoo, and H. Matsunami, J. Appl. Phys. **73**, 726 (1993).
8. T. Kimoto and H. Matsunami, J. Appl. Phys. **76**, 7322 (1994).
9. D.J. Larkin, P.G. Neudeck, J.A. Powell, and L.G. Matus, Appl. Phys. Lett. **65**, 1659 (1994).
10. H. S. Kong, J.T. Glass, and R.F. Davis, J. Appl. Phys. **64**, 2672 (1988).
11. P. Liaw and R.F. Davis, J. Electrochem. Soc. **132**, 642 (1985).
12. J. A. Powell, L. G. Matus, and M.A. Kuczmarski, J. Electrochem. Soc. **134**, 1558 (1987).

H_2 and Silicon

13. G. Schulze and M. Henzler, Surface Science **124**, 336 (1983).
14. L.H. Chua, R.B. Jackman, and J.S. Foord, Surface Science **315**, 69 (1994).
15. S.M. Gates and S.K. Kulkarni, Appl. Phys. Lett. **60**, 53 (1992).
16. B.G. Koehler, C.H. Mak, D.A. Arthur, P.A. Coon, and S.M. George, J. Chem. Phys. **89**, 1709 (1988).
17. C.C. Cheng, S.R. Lucas, H. Gutleben, W.J. Choyke, and J.T. Yates, J. Am. Chem. Soc. **114**, 1249 (1992).
18. S.M. Gates, R.R. Kunz, and C.M. Greenlief, Surface Science **207**, 364 (1989).
19. M. Liehr, C.M. Greenlief, M. Offenberg, and S.R. Kasi, J. Vac. Sci. Technol. A **8**, 2960 (1990).
20. J.J. Boland, Phys. Rev. Lett. **65**, 3325 (1990).
21. R.M. Wallace, P.A. Taylor, W.J. Choyke, and J.T. Yates, Surface Science **239**, 1 (1990).
22. H. Kobayashi, K. Edamoto, M. Onchi, and M. Nishijima, J. Chem. Phys. **78**, 7429 (1983).
23. K. Sinniah, M.G. Sherman, L.B. Lewis, W.H. Weinberg, J.T. Yates, and K.C. Janda, J. Chem. Phys. **92**, 5700 (1990).
24. C.M. Greenlief, S.M. Gates, and P.A. Holbert, Chem. Phys. Lett. **159**, 202 (1989).
25. M.K. Farnaam and D.R. Olander, Surface Science **145**, 390 (1984).
26. D. Ludden, R. Tsu, T.R. Bramblett, and J.E. Greene, J. Vac. Sci. Technol. A **9**, 3003 (1991).
27. S.M. Gates, C.M. Greenlief, and D.B. Beach, J. Chem. Phys. **93**, 7493 (1990).
28. J.S. Montgomery, T.P. Schneider, R.J. Carter, J.P. Barnak, Y.L. Chen, J.R. Hauser, and R.J. Nemanich, Appl. Phys. Lett. **67**, 2194 (1995).

29. K. Nakashima, M. Ishii, I. Tajima, and M. Yamamoto, Appl. Phys. Lett. **58**, 2663 (1991).
30. Y. Morita and H. Tokumoto, Appl. Phys. Lett. **67**, 2654 (1995).
31. C. Kleint and K.D. Brzoska, Surface Science **231**, 177 (1990).

Hydrogen and Diamond
32. A.V. Hamza, G.D. Kubiak, and R.H. Stulen, Surface Science **237**, 35 (1990).
33. V.S. Smentkowski, H. Jansch, M.A. Henderson, and J.T. Yates, Surface Science **330**, 207 (1995).
34. R.E. Thomas, R.A. Rudder, and R.J. Markunas, J. Vac. Sci. Technol. A **10**, 2451 (1992).
35. B. Pate, Surface Science **165**, 83 (1986).
36. S. Matsumoto, Y. Sato, and N. Setaka, Carbon **19**, 234, (1981).
37. O.M. Kuttel, L. Diederich, E. Schaller, O. Carnal, and L. Schlapbach, Surface Science **337**, L812 (1995).
38. Y. Mitsuda, T. Yamada, T.J. Chuang, H. Seki, R.P. Chin, J.Y. Huang, and Y.R. Shen, Surface Science Letters **257**, L633 (1991).
39. L.H. Chua, R.B. Jackman, J.S. Foord, P.R. Chalker, C. Johnston, and S. Romani, J. Vac. Sci. Technol. A **12**, 3033 (1994).
40. T. Ando, M. Ishii, M. Kamo, and Y. Sato, J. Chem. Soc. Faraday Trans. **89**, 1783 (1993).
41. J. van der Weide and R.J. Nemanich, Appl. Phys. Lett. **62**, 1878 (1993).

Hydrogen and GaAs and InP
42. G.V. Jagannathan, M.L. Andrews, and A.T. Habig, Appl. Phys. Lett. **56**, 2019 (1990).
43. I. Suemune, Y. Kunitsugu, Y. Tanaka, Y. Kan, and M. Yamanishi, Appl. Phys. Lett. **53**, 2173 (1988).
44. M. Yamada and Y. Ide, Jpn. J. Appl. Phys. **33**, L671 (1994).
45. C.M. Rouleau and R.M. Park, J. Appl. Phys. **73**, 4610 (1993).
46. Y. Sakamoto, T. Sugino, H. Ninomiya, K. Matsuda, and J. Shirafuji, Jpn. J. Appl. Phys. **34**, 1417 (1995).

Hydrogen and SiC
47. M.D. Allendorf and D.A. Outka, Surface Science **258**, 177 (1991).
48. Y. Kim and D.R. Olander, Surface Science **313**, 399 (1994).
49. J.M. Lannon, J.S. Gold, and C.D. Stinespring **77**, 3823 (1995).
50. A.O. Konstantinov, N.S. Konstantinova, O.I. Kon'kov, E.I. Terukov, and P.A. Ivanov, Semiconductors **28**, 209 (1994).
51. M.E. Lin, S. Strite, A. Agarwal, A. Salvador, G.L. Zhou, N. Teraguchi, A. Rockett, and H. Morkoc, Appl. Phys. Lett. **62**, 702 (1993).

SiC/III-N Devices
52. R.F. Davis, Advances in Ceramics **23**, 477 (1987).
53. R.F. Davis, G. Kelner, M. Shur, J. Palmour, J.A. Edmond, Proc. of the IEEE **79**, 677 (1991).
54. S. Strite and H. Morkoc, J. Vac. Sci. Technol. B **10**, 1237 (1992).

H_2 Thermal Etching
55. T.L. Chu and R.B. Campbell, J. Electrochem. Soc. **112**, 955 (1965).
56. J.M. Harris, H.C. Gatos, and A.F. Witt, J. Electrochem. Soc. **116**, 380 (1969).
57. R.W. Bartlett and R.A. Mueller, Mat. Res. Bull. **4**, S341 (1969).
58. D. Kim and D. Choi, J. Am. Ceram. Soc. **79**, 503 (1996).

H and H_2 Ion Implantation/Sputtering
59. J. Bohdansky and J. Roth, J. Nucl. Mater. **122/123**, 1417 (1984).
60. U.R. Ajerk, J. Irr. Results **1**, 23 (1997).

61. K. Sone, M. Saidoh, K. Nakamura, R. Yamada, Y. Muragami, T. Shikama, M. Fukutomi, M. Kitajima, and M. Okada, J. Nucl. Mater. **98**, 270 (1981).
62. M. Mohri, K. Watanabe, and T. Yamashina, J. Nucl. Mater. **75**, 7 (1978).
63. T. Yamashina, M. Mohri, K. Watanabe, H. Doi, and K. Hayakawa, J. Nucl. Mater. **76/77**, 202 (1978).
64. J. Bohdansky, H.L. Bay and W. Ottenberg, J. Nucl. Mater. **76/77**, 163 (1978).
65. D. Keroack and B. Terreault, J. Vac. Sci. Technol. A **14**, 3130 (1996).

(3×3) 6H-SiC $(0001)_{Si}$ Surfaces and Characterization
66. R. Kaplan and T.M. Parrill, Surface Science **165**, L45 (1986).
67. R. Kaplan, Surface Science **215**, 111 (1989).
68. V.M. Bermudez, Appl. Surf. Sci. **84**, 45 (1995).
69. S. Nakanishi, H. Tokutaka, K. Nishimori, S. Kishida, and N. Ishihara, Appl. Surf. Sci. **41/42**, 44 (1989).
70. V. van Elsbergen, T.U. Kampen, and W. Monch, Surface Science **365**, 443 (1996).
71. L. Li and I.S.T. Tsong, Surface Science **351**, 141 (1996).
72. M.A. Kulakov, G. Henn, and B. Bullemer, Surface Science **346**, 49 (1996).
73. R.S. Kern, Ph.D. dissertation, NCSU (1996).
74. A. Fissel, U. Kaiser, E. Ducke, B. Schroter, and W. Richter, J. Cryst. Growth **154**, 72 (1995).
75. A. Fissel, B. Schroter, and W. Richter, Appl. Phys. Lett. **66**, 3182 (1995).
76. S.W. King, M.C. Benjamin, R.S. Kern, D. Hanser, J.P. Barnak, R.J. Nemanich, and R.F. Davis, submitted to J. Appl. Phys..
77. M.C. Benjamin, S.W. King, J.P. Barnak, R.S. Kern, R.F. Davis, and R.J. Nemanich, submitted to J. Appl. Phys..
78. H. Kim, G. Glass, S.Y. Park, T. Spila, N. Taylor, J.R. Abelson, and J.E. Greene, Appl. Phys. Lett. **69**, 3869 (1996).

Experimental Information
79. J. van der Weide, Ph.D. Dissertation, NCSU.
80. V.S. Smentkowski and J.T. Yates, Jr., J. Vac. Sci. Technol. A, 7 3325 (1989).
81. Perkin Elmer XPS Handbook.
82. J.A. Kalomiros, E.C. Paloura, A. Ginoudi, S. Kennou, S. Ladas, Ch. Lioutas, N. Vouroutzis, G. Voutsas, D. Girginoudi, N. Georgoulas, and A. Thanailakis, Solid State Comm. **96**, 735 (1995).
83. B.M.H. Ning and J.E. Crowell, Surface Science **295**, 79 (1993).
84. N.M. Russell and J.G. Ekerdt, Surface Science **369**, 51 (1996).
85. L. Surnev and M. Tikhov, Surface Science **138**, 40 (1984).

Surface Diffusion
86. A. Vittadini, A. Selloni, and M. Casarin, Surface Science **289**, L625 (1993).
87. G.A. Reider, U. Hofer, and T.F. Heinz, Phys. Rev. Lett. **66**, 1994 (1991).
88. G. Li, Y.C. Chang, R. Tsu, and J.E. Greene, Surface Science **330**, 20 (1995).
89. B. Voigtlander and A. Zinner, Surface Science **292**, L775 (1993).
90. K.N. Tu, J.W. Mayer, L.C. Feldman, Electronic Thin Film Science for Electrical Engineers and Materials Scientists, pg 132 (1987). Macmillan Pub. Co., New York.
91. T. Kimoto and H. Matsunami, J. Appl. Phys. **78**, 3132 (1995).
92. T. Kimoto and H. Matsunami, J. Appl. Phys. **75**, 850 (1994).
93. T. Takai, T. Halicioglu, and W.A. Tiller, Surface Science **164**, 327 (1985).
94. M.T. Schulberg, M.D. Allendorf, and D.A. Outka, Surface Science **341**, 262 (1995).
95. M.V. Ascherl, J.H. Campbell, J. Lozano, and J.H. Craig, Jr., J. Vac. Sci. Technol. A **13**, 2721 (1995).
96. S.W. King, R.J. Nemanich, and R.F. Davis, submitted to the J. Electrochem. Soc.
97. B. Douglas, D.H. McDaniel, and J.J. Alexander, Concepts and Models of Inorganic Chemistry, p. 74, John Wiley & Sons, New York, (1983).

V. Distribution List

Dr. Colin Wood Office of Naval Research Electronics Division, Code: 312 Ballston Tower One 800 N. Quincy Street Arlington, VA 22217-5660	3
Administrative Contracting Officer Office of Naval Research Atlanta Regional Office 100 Alabama Street, Suite 4R15 Atlanta, GA 30303	1
Director, Naval Research Laboratory ATTN: Code 2627 Washington, DC 20375	1
Defense Technical Information Center 8725 John J. Kingman Road Suite 0944 Ft. Belvoir, VA 22060-6218	2